

NASA  
CR  
3032  
c.1

# NASA Contractor Report 3032

TECH LIBRARY KAFB, NM  
0061844

LOAN COPY RE  
AEWL TECHNICAL  
KIRTLAND AFB

## Experimental Study of the Effect of Cycle Pressure on Lean Combustion Emissions

Gerald Roffe and K. S. Venkataramani

CONTRACT NAS3-20581  
JULY 1978





## NASA Contractor Report 3032

# Experimental Study of the Effect of Cycle Pressure on Lean Combustion Emissions

Gerald Roffe and K. S. Venkataramani  
*General Applied Science Laboratories, Inc.*  
*Westbury, New York*

Prepared for  
Lewis Research Center  
under Contract NAS3-20581

**NASA**

National Aeronautics  
and Space Administration

**Scientific and Technical  
Information Office**

1978



## TABLE OF CONTENTS

	<u>Page</u>
SUMMARY	1
INTRODUCTION	2
APPARATUS AND PROCEDURES	3
RESULTS	13
DISCUSSION	23
SUMMARY OF RESULTS	33
APPENDIX A - DATA REDUCTION PROCEDURES	34
APPENDIX B - DATA SUMMARY	38

## SUMMARY

Experiments were conducted in which a stream of premixed propane and air was burned in a flametube apparatus under conditions representative of gas turbine operation. Emissions of  $\text{NO}_x$ , CO and unburned hydrocarbons were measured over a range of inlet temperature from 600K to 1000K, pressure from 5 atm to 30 atm and combustor residence time from 1msec to 3msec at equivalence ratios from 0.7 down to the lean stability limit.

At an inlet temperature of 800K,  $\text{NO}_x$  emission index data was well represented by curves of the form  $E_{\text{NO}_x} \sim \sqrt{P}$ . Data at 1000K inlet temperature were insufficient to define a pressure trend. At an inlet temperature of 600K observed  $\text{NO}_x$  levels dropped markedly with decreasing pressure for pressures below 20 atm. For a fixed pressure,  $\text{NO}_x$  level was found to be principally a function of adiabatic flame temperature with this parameter combining the individual effects of inlet temperature and equivalence ratio.  $\text{NO}_x$  emission index was observed to increase linearly with combustor residence time.

CO levels were found to have peaked at some point prior to the first measurement at 1 msec combustor residence time and to decrease steadily with time until an equilibrium condition is attained. For adiabatic flame temperatures of 2050K and higher, CO was found to reach equilibrium within 2 msec.

Unburned hydrocarbon species dropped to a negligible level within 2 msec regardless of inlet temperature, pressure or equivalence ratio. Increasing adiabatic flame temperature increased the rate of destruction of UHC species. For a combustor residence time of 2.5 msec, combustion inefficiency fell below 0.01% at an adiabatic flame temperature of 2050K as a result of the disappearance of UHC species and the equilibration of CO. The maximum combustion inefficiency observed in this fully gas phase combustion system was on the order of 1% and occurred just before the lean flameout condition (lean stability limit).

Using a perforated plate flameholder, the lean stability limit is well represented by the condition of 1800K adiabatic flame temperature. There is a small effect of inlet temperature with excursions of  $\pm 200\text{K}$  in this variable causing the stability limit to vary by  $\mp 50\text{K}$ .

## INTRODUCTION

Recent experiments have indicated considerable potential for the lean premixed-prevaporized (LPP) combustion technique as a means of producing high efficiency combustion with oxides of nitrogen emission levels far lower than those corresponding to conventional combustion processes. As applied to gas turbine design, interest in LPP combustion has focused on the stratospheric cruise condition where the combustor pressure is typically between four and six atmospheres and combustor inlet temperature is approximately 800K, since high  $\text{NO}_x$  emissions at stratospheric altitudes may be capable of causing environmental damage. However, the control of gas turbine emissions is a recognized goal which applies over the entire spectrum of operating conditions. It is, therefore, necessary to assess the capabilities of the LPP combustion technique over the range of conditions representative of aircraft gas turbine operation. A meaningful lower bound, and therefore, design objective is obtained by establishing the emission indices for well premixed gas phase systems as a function of cycle pressure, temperature and equivalence ratio for fixed values of combustor residence time. This is the main objective of the research program described here.

This report describes an experimental program in which a well mixed stream of gaseous propane and air with a reference velocity of 25m/sec was passed through a perforated plate flameholder and burned in a flametube apparatus at pressures of 5, 10, 20 and 30 atmospheres and inlet temperature of 600K, 800K and 1000K. Emission indices were measured for oxides of nitrogen ( $\text{NO}_x$ ), carbon monoxide (CO) and unburned hydrocarbons (UHC) at combustor residence times from one to three milliseconds and equivalence ratios from 0.7 to the lean stability limit.

## APPARATUS AND PROCEDURES

### Combustion Test Rig

The basic aim of this program is the acquisition of emissions data for pre-mixed gas-phase hydrocarbon/air combustion systems at pressures up to 30 atm and temperatures up to 1000K under flow conditions representative of those which might be encountered in an aircraft gas turbine engine. To assure a gas phase mixture, regardless of pressure, propane was selected as the test fuel and heated to a temperature of 380K (slightly in excess of its critical temperature) prior to injection to eliminate the possibility of liquid phase fuel entering the apparatus.

In an effort to keep flow conditions in the device as similar as possible to those in an operational engine, the mixer tube reference velocity was set at 25m/sec. Since predicted chemical reaction times for propane air systems are short compared with the one to three millisecond combustor residence times of interest in gas turbine applications, an instantaneous rise in temperature can be assumed in the combustor, leading to a maximum length requirement of 27 cm for a residence time of 3msec at the 600K inlet temperature condition and equivalence ratio 0.7. In order to minimize wall effects, a single gas sample can be withdrawn at the combustor centerline, but the combustor length to diameter ratio must be kept small (between three and four) to prevent gas from the regions of wall influence from diffusing to the centerline sampling position. A combustor diameter of 7.9 cm was selected as meeting the length to diameter ratio criterion and corresponding to a standard commercial size.

One of the principal problems to be overcome in the design of the experiment was that of producing a uniform fuel/air mixture within the constraints placed by autoignition time at the high temperatures and pressures of interest here. Ignition delay data for propane air systems is currently available only at pressures near one atmosphere. However, the observed pressure dependence can be used to extrapolate available results to a 30 atm - 1000K operating point goal and restricts fuel residence time in the mixing region to no more than 10 msec. Combining this constraint with the 25 m/sec reference velocity chosen for the experiment leads to a fuel/air mixing length restriction of

25 cm. In order to achieve good mixing in a length amounting to approximately three mixer tube diameters, a large number of fuel injection points were employed. The apparatus used fifty-two injection tubes (one injector per square centimeter of mixer area) spraying fuel in the streamwise direction in order to produce mixing streamtubes with length to diameter ratios of twenty in order to achieve adequate mixing within the distance available. Adequate mixing was defined as a fuel/air distribution profile at the combustor entrance with local deviations of no more than 10% from a perfectly mixed condition.

The combustion test rig is illustrated schematically in Figure (1). Heated dry air enters the apparatus through the bellmouth, passing through an instrumentation spool where the entrance temperature and pitot-static pressure profiles are measured by an embedded rake. Fuel enters the device by means of a plenum chamber which surrounds the instrumentation spool and feeds fifty-two individual 1.6 mm diameter injection tubes. The tubes extend 7 cm downstream from their entry point and inject fuel in the streamwise direction in order to minimize the possibility of local flow separation. The relatively long and thin injection tubes are supported at their midpoints by a fine (0.05 mm web thickness) honeycomb structure 6mm in streamwise extent representing a flow blockage of 3%. The fuel injector assembly is shown in Figure (2).

The mixer tube was constructed of a heavy outer pressure wall and a thin stainless steel liner. The two elements were separated by an internally vented air gap to minimize heat loss. Two thermocouples were mounted 180° apart 2.5 cm from the downstream end of the mixer and placed so that their tips were flush with the inner surface of the liner. The thermocouples served as indicators of autoignition in the mixer or flashback through the flameholder.

The flameholder assembly is illustrated in Figure (3). The flameholder is a water-cooled perforated plate, employing 21 holes 0.95 cm in diameter to produce a porosity of 22%. The flameholder produced a total pressure drop of approximately 3%. It is provided with two wall surface thermocouples on the downstream surface and one on the upstream surface and an integral hydrogen-air igniter which is used to initiate combustion. Flameholder depth, measured in the streamwise direction, is 1.6 cm.



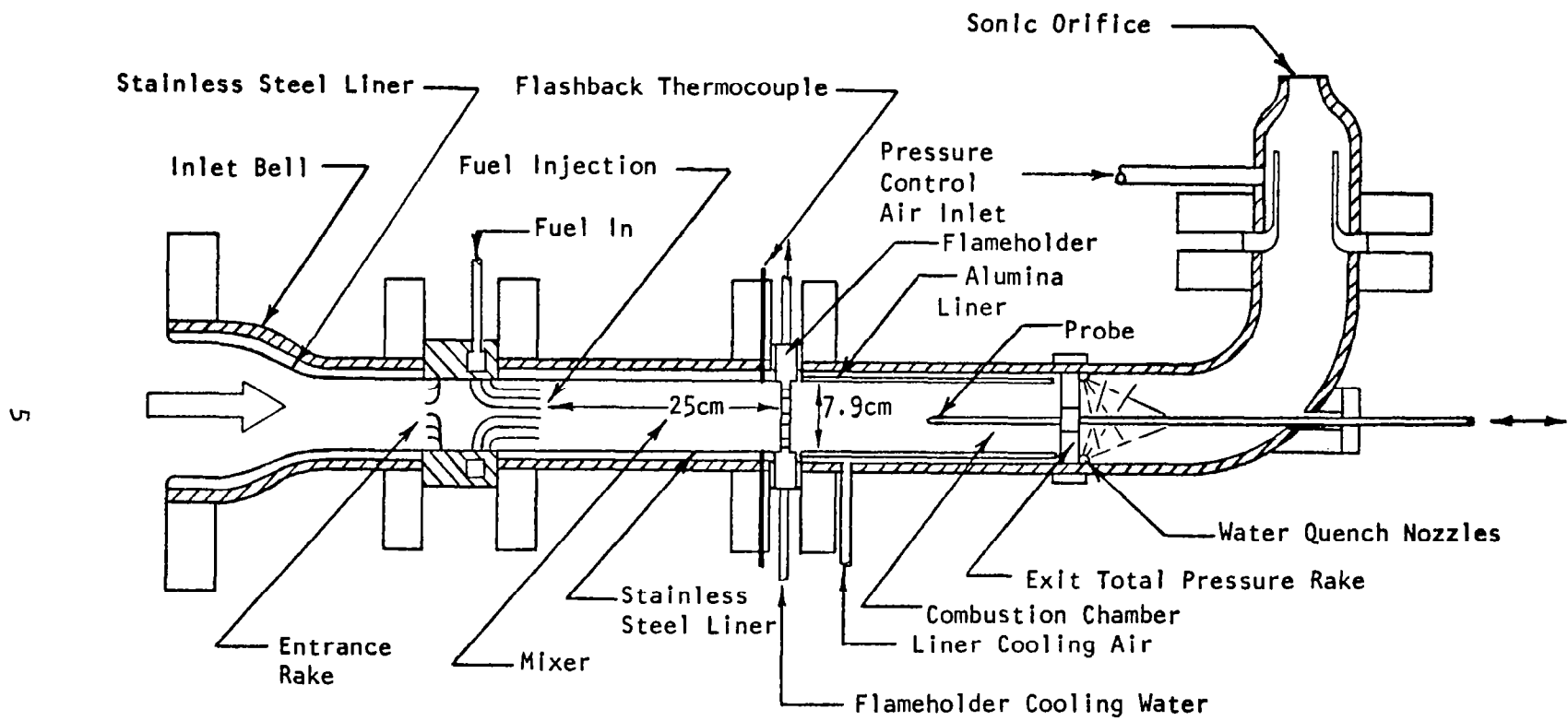


FIGURE 1. COMBUSTION TEST RIG

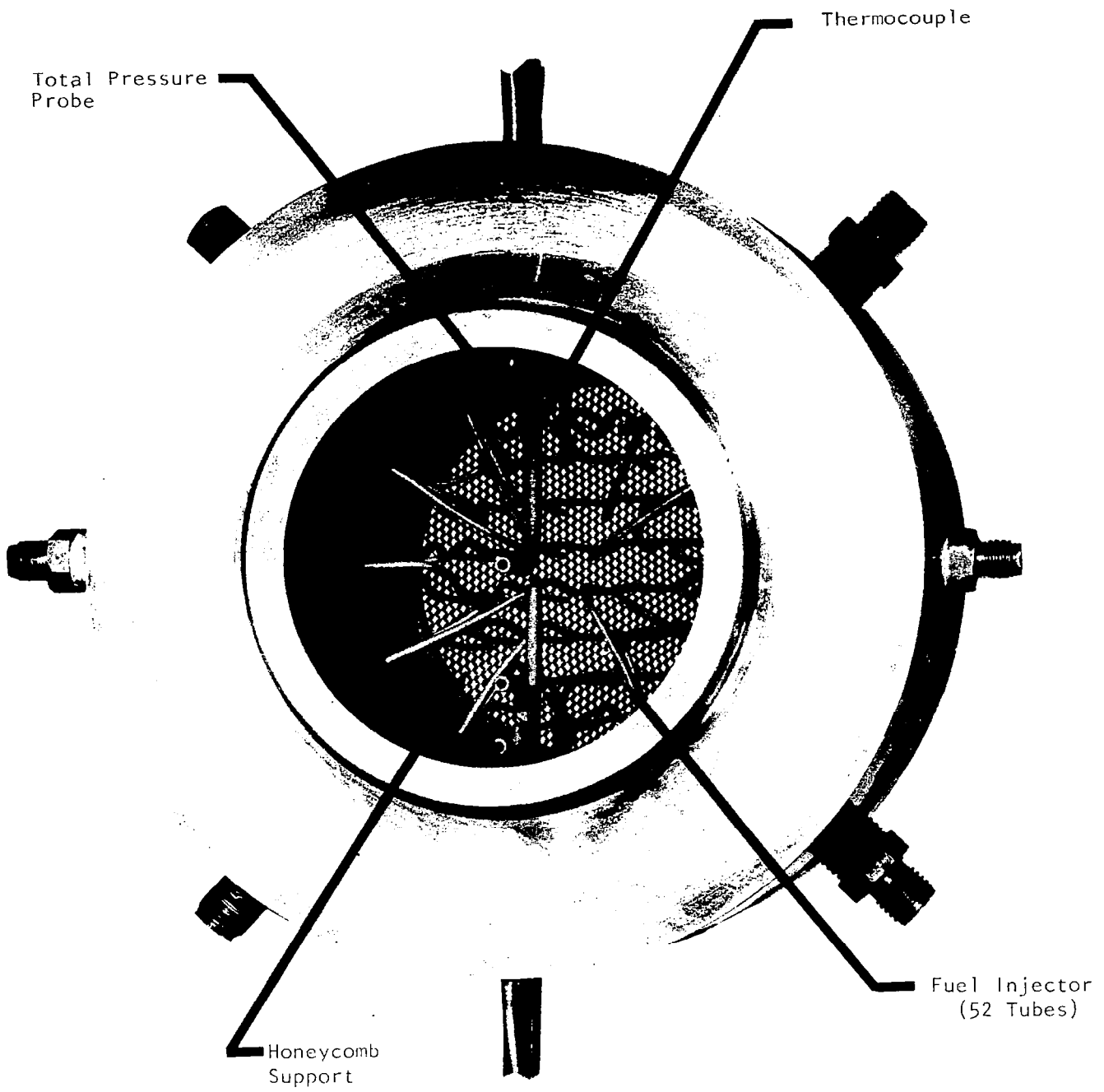


FIGURE 2. FUEL INJECTOR ASSEMBLY (VIEWED FROM UPSTREAM SIDE)

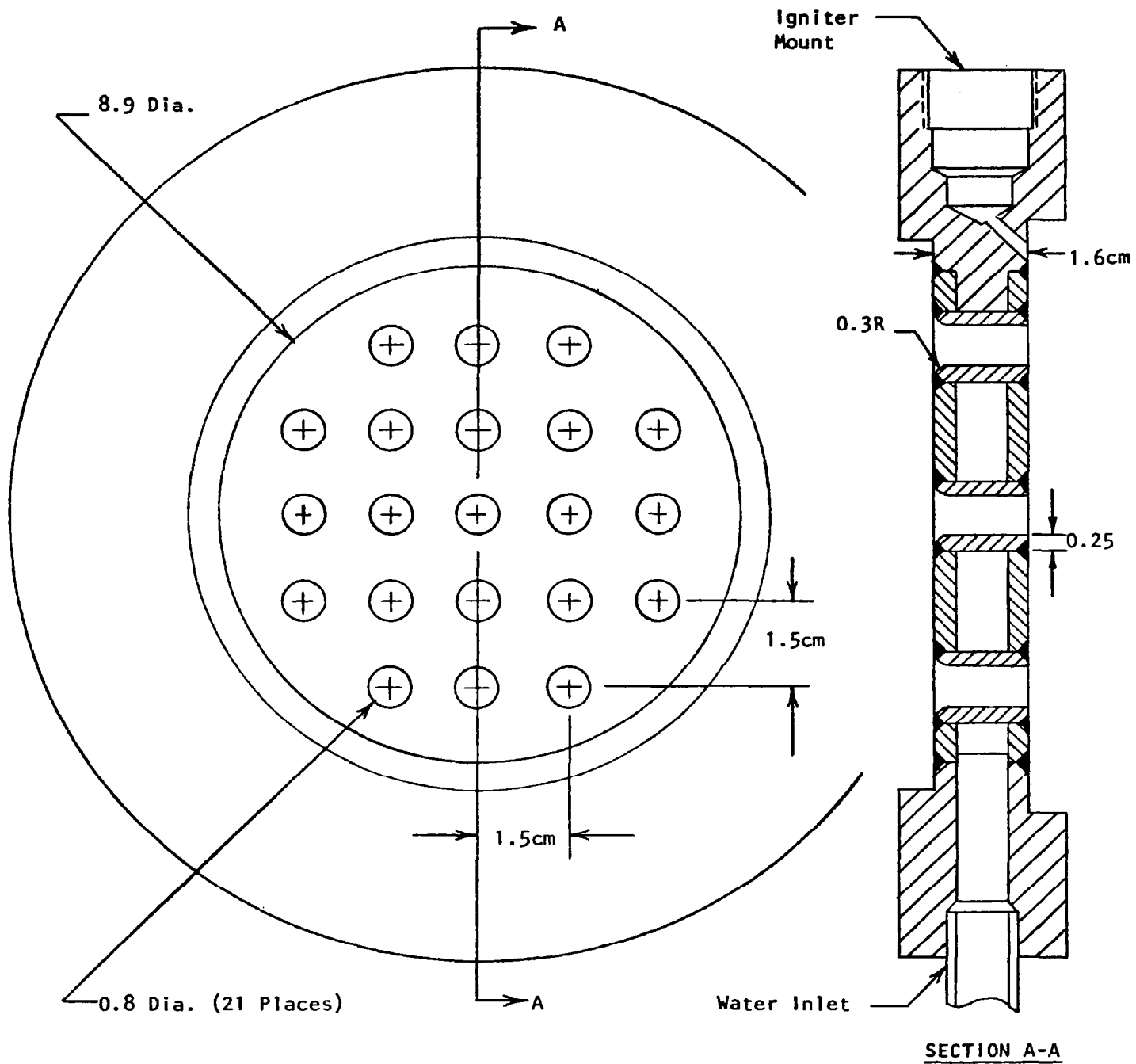


FIGURE 3. WATER-COOLED PERFORATED PLATE FLAMEHOLDER

The combustor assembly also employed a double wall design to protect the heavy outer pressure wall. However, here the air gap between the combustor liner and the outer wall was kept cool by injecting a small amount of cold air. In addition, an alumina tube was mounted inside the stainless steel liner to provide an uncooled refractory combustor wall, minimizing radiation losses from the gas.

A dome-loaded pressure regulator was used to supply cold air to an annular injection section just upstream of the rig exit orifice. By loading the regulator to the pressure desired for the test, the appropriate amount of cold air is added automatically to produce the correct total pressure in the test rig. This method of pressure control offers the dual advantages of automatic compensation for varying combustor exit temperature and thermal protection for the choked exit orifice.

#### Instrumentation

During emissions testing, gas samples were withdrawn from the combustor using the water-cooled sampling probe illustrated in Figure (4). The probe is 1.2 cm in diameter and is provided with a 1.6 mm entrance port. The high pressures and flame temperatures of interest in this program constitute a difficult problem with regard to gas sample quenching. The problem is particularly severe in the case of carbon monoxide whose oxidation reactions are pressure accelerated and speeded by the high OH concentrations typical of these flames. The difficulty here is associated with the sample quenching process. As the sample is cooled, the equilibrium concentration of CO decreases. If the sample quenching rate is too slow, CO levels will drop during the cooling process, attempting to remain in equilibrium. In order to minimize the reactions in the probe, a two-step sample quench process was employed. First, the sample gas was expanded into a 6mm diameter dump tube within which the pressure was maintained at just under 5 atm, regardless of combustor operating pressure. A portion of this lower pressure sample was thermally quenched by withdrawing it through a 1.6mm tube immersed in the probe cooling water.

The entire probe assembly was movable and used to withdraw gas samples at locations corresponding to desired residence times within the combustor. Residence time for a given axial position was calculated based on an assumed

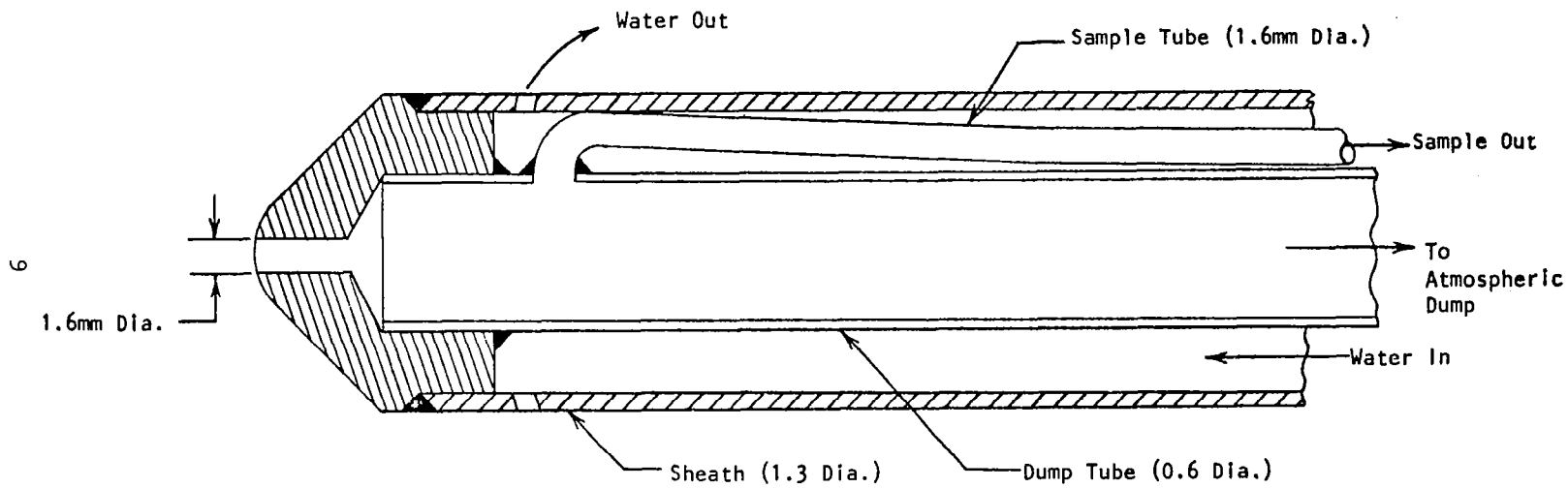


FIGURE 4. PRESSURE REDUCTION SAMPLING PROBE

instantaneous rise from the mixer temperature to the adiabatic flame temperature. The rather long sample probe was supported at the exit of the ceramic lined combustor section by a water-cooled strut which served as the housing for an array of total pressure tubes which were used to measure the total pressure drop of the combustor.

Prior to performing emissions testing, it was necessary to assure that the apparatus was producing a sufficiently uniform mixture of fuel and air, defined for this program as a maximum local deviation of no more than 10% from the perfectly mixed condition. To do this, a sampling rake was positioned 2 cm downstream of the flameholder and gas samples were withdrawn at seven points across the combustor diameter. The gas samples were passed through a catalytic reactor which converted incompletely oxidized fuel species to  $\text{CO}_2$  and water. The catalytically reacted samples were then processed by the gas analysis system to determine their fuel/air ratio.

#### Fuel System and Properties

The fuel supply system is illustrated in Figure (5). Liquid propane is stored in a tank pressurized with nitrogen. The liquid is withdrawn from the lower section of the supply tank, passing through a turbine flowmeter and pressure regulator before entering a cavitating venturi which provides a constant fuel mass flow rate independent of downstream pressure fluctuations. Fuel flow rate is controlled during a test by adjusting the regulated pressure on the upstream side of the cavitating venturi. The propane is heated to a temperature of 380K in a pressurized water bath and passed through a heated line to a metering venturi before being delivered to the injection plenum. Typical analyses of the commercial grade propane used in these experiments are presented in Table I (page 11).

#### Test Procedure

In operation, the air flow through the rig was first established at the desired temperature and at a mass flow rate corresponding to the 25 m/sec reference velocity at the test pressure and temperature. The rig pressure was then brought up to the operating value by injection of an appropriate amount of cold air at

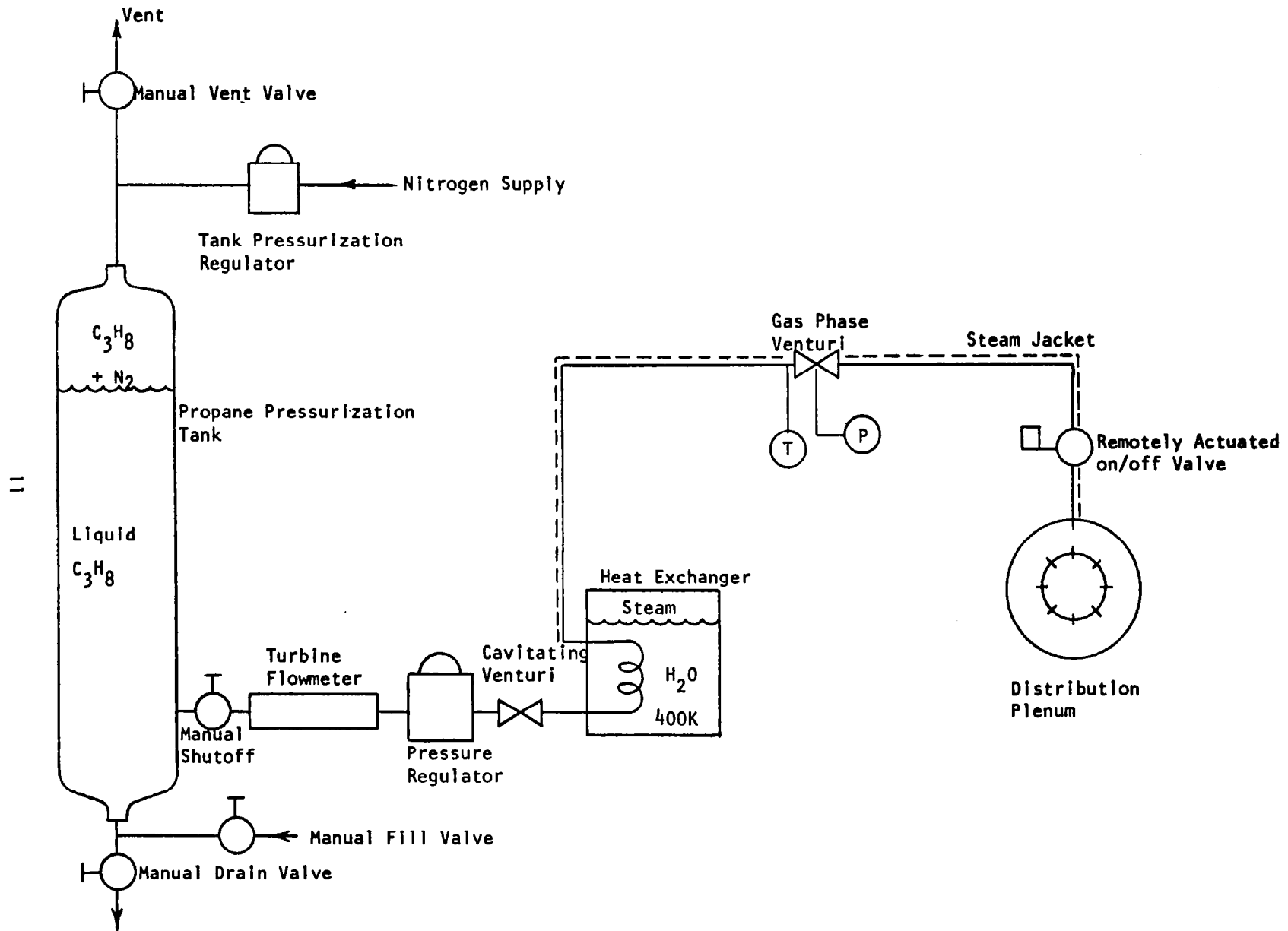


FIGURE 5. PROPANE STORAGE AND DELIVERY SYSTEM SCHEMATIC

the exit orifice. The gas igniter was turned on, fuel flow was initiated and slowly increased until ignition was achieved. The rig equivalence ratio was brought to the highest level desired during the particular test sequence, the gas igniter shut off and the rig operated for several minutes to assure steady conditions. Gas samples were then withdrawn at a series of combustor locations corresponding to various residence times between one and three milliseconds. Once a residence time scan had been completed, the equivalence ratio was lowered and the procedure repeated. Continuing to lower the equivalence ratio eventually caused the flame to blow out. Conditions at this point were defined as those corresponding to the lean stability limit.

The gas sample withdrawn from the combustor was analyzed using equipment and procedures conforming to SAE ARP 1256. The details of the gas analysis system and data reduction equations are presented in Appendix A.

TABLE I

Analysis of Commercial Grade Propane Used in Test Program

Property	Sample 1	Sample 2
% Propane	95.3	99.1
% Butane	0.04	0.50
% Ethylene and Ethane	0.004	0.20
% Propylene	4.66	0.20
Volitile sulfur, ppm	<0.5	<0.5
Specific gravity (air = 1.0)	1.55	1.55
Vapor pressure (KPa @ 20°C)	837	830
Hydrogen/carbon ratio	2.64	2.67



## RESULTS

Figure (6) presents the results of fuel distribution tests carried out at an inlet temperature of 800K and pressures of 5, 10 and 20 atm. The maximum local deviation of measured fuel/air ratio from the mean (or perfectly mixed value) decreases from 9% at the 5 atm condition to 5% at 10 atm and 4% at 20 atm. The r.m.s. deviation of the fuel distribution profiles from the mean was 5.5% at 5 atm, 2.4% at 10 atm and 2.3% at 20 atm. Fuel distribution tests were not run at pressures higher than 20 atm but the trend in the data is toward greater uniformity as the mass flow (and injector pressure drop) increases.

Table II summarizes the matrix of pressure ( $P_3$ ) - inlet temperature ( $T_3$ ) operating conditions covered in this program. Matrix points indicated by a star denote conditions at which emissions data were taken. At the two

TABLE II  
Summary of Operating Conditions

$P_3 \backslash T_3$	600K	800K	1000K
5 atm	*	*	*
10 atm	*	*	*
20 atm	*	*	F
30 atm	U	*	F

matrix points marked with the symbol "F", flashback into the mixer occurred upon ignition in the combustor and it was not possible to obtain emissions data. Operation at the 30 atm - 600K corner of the matrix produced unstable combustion, denoted by the symbol "U". This instability manifested itself as large pressure fluctuations or a chugging phenomenon. It was possible to operate the device over a very small range of equivalence ratio normally falling below the lean stability limit by artificially stabilizing the flame with the gas igniter. A complete tabulation of all emissions data will be found in Appendix B.

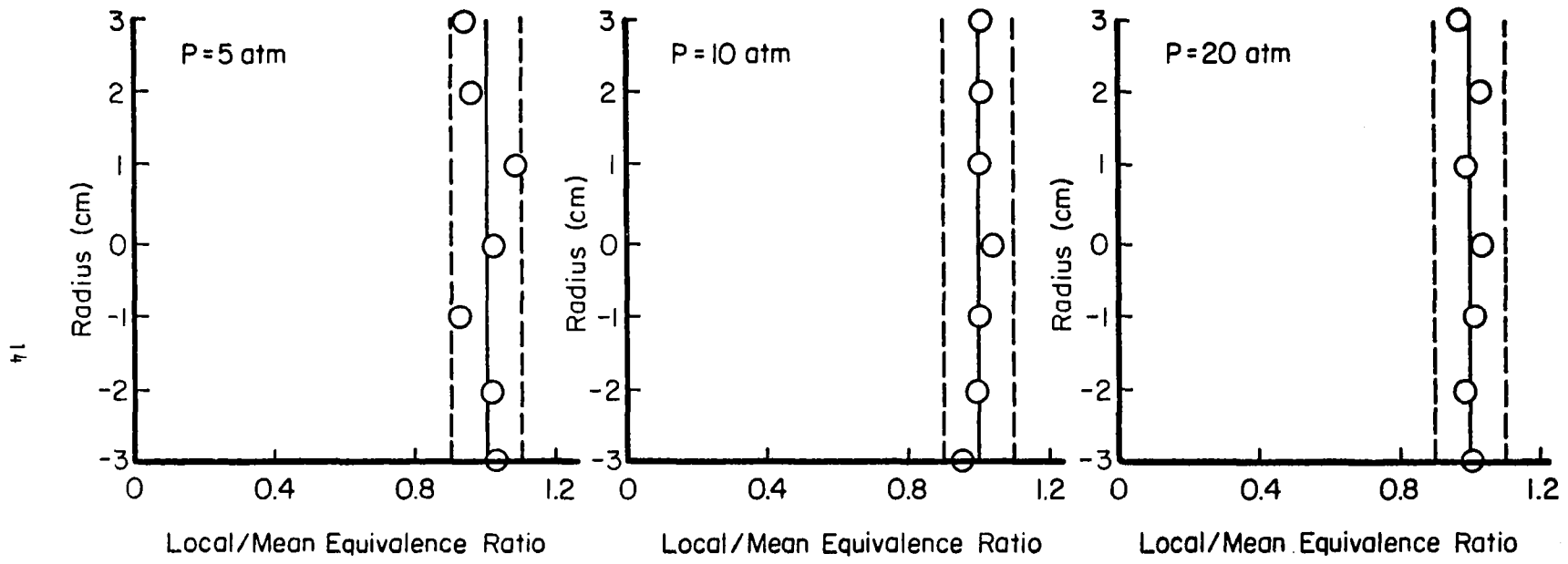


FIGURE 6. RADIAL FUEL DISTRIBUTIONS 2 CM DOWNSTREAM OF FLAMEHOLDER ( $T_3 = 800K$ ,  $\phi = 0.6$ )

Figures (7) and (8) present the measured emission indices for  $\text{NO}_x$  and CO over the pressure-inlet temperature matrix for a combustor residence time of two milliseconds. Equivalence ratio is calculated from measured exhaust gas concentrations following the method described in Appendix A. Any data for which the equivalence ratio derived from chemical analysis differed by more than  $\pm 15\%$  from that obtained from air and fuel mass flow measurements was not used.

The qualitative behavior of both  $\text{NO}_x$  and CO emission index is in agreement with previous low pressure data.  $\text{NO}_x$  emissions increase exponentially with increasing equivalence ratio, but drop off rapidly near the lean stability limit. CO emissions are high near the lean stability limit, drop off as equivalence ratio increases, reach a minimum and then begin to rise in apparent response to the shifting composition required for chemical equilibrium.

The measured emission indices for  $\text{NO}_x$ , CO and unburned hydrocarbons are presented in Figure (9) as functions of combustor residence time. Hydrocarbon oxidation is completed early with trace hydrocarbon species rarely measurable after 1.5 msec. Carbon monoxide levels peak sometime between zero and one millisecond, drop very rapidly between one and two milliseconds and, in most cases, do not vary appreciably from that point on.

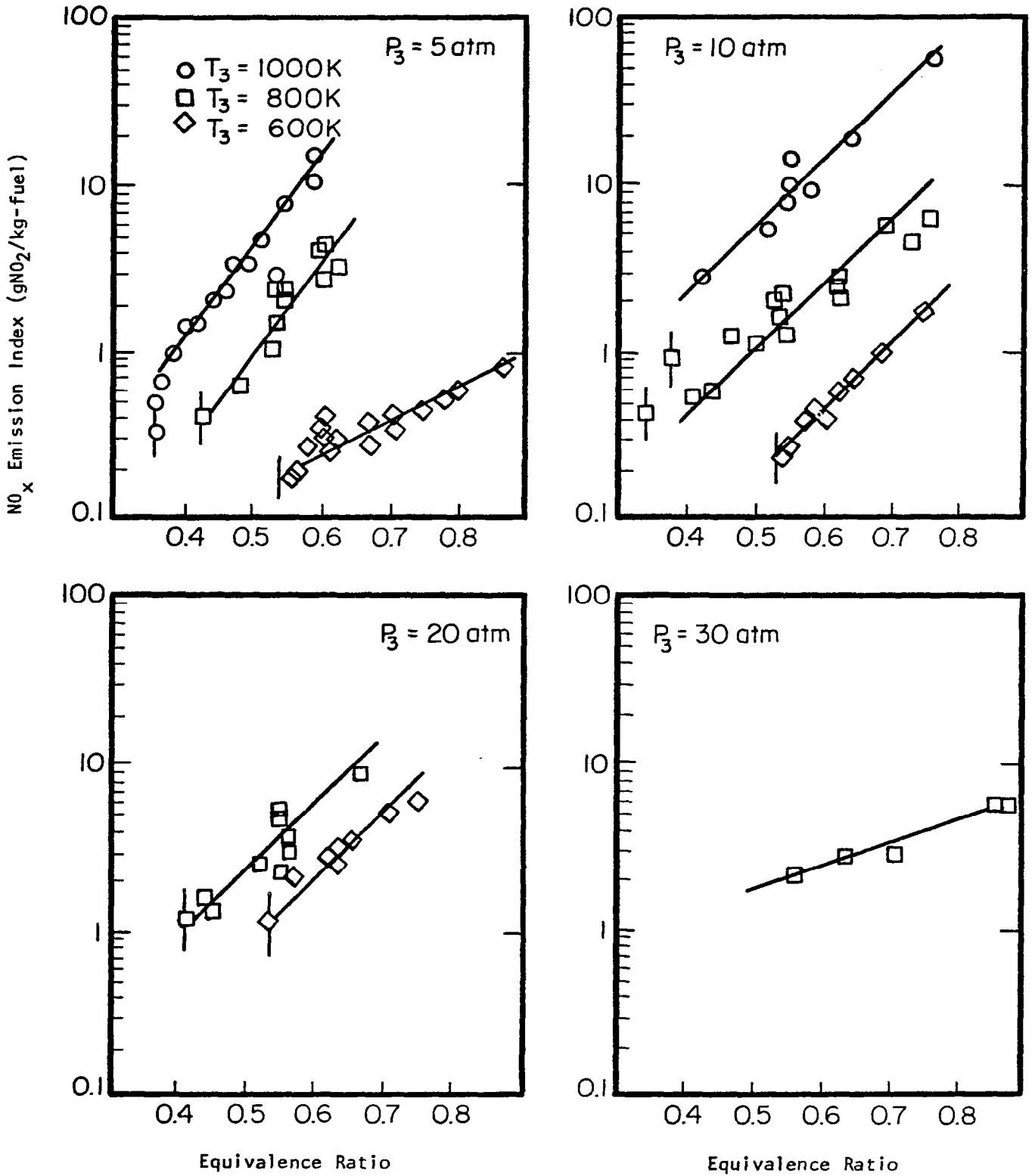


FIGURE 7.  $\text{NO}_x$  EMISSION INDEX FOR 2 MSEC COMBUSTOR RESIDENCE TIME

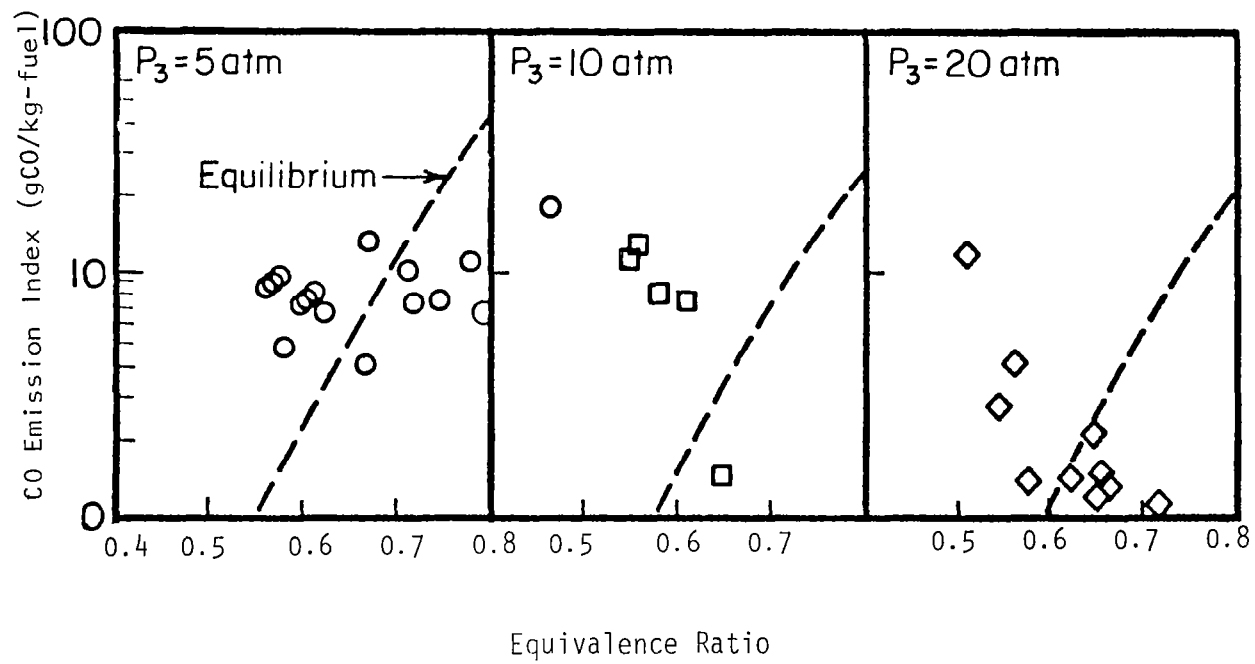


FIGURE 8a. CO EMISSION INDEX FOR 2 MSEC COMBUSTOR RESIDENCE TIME ( $T_3=600K$ )

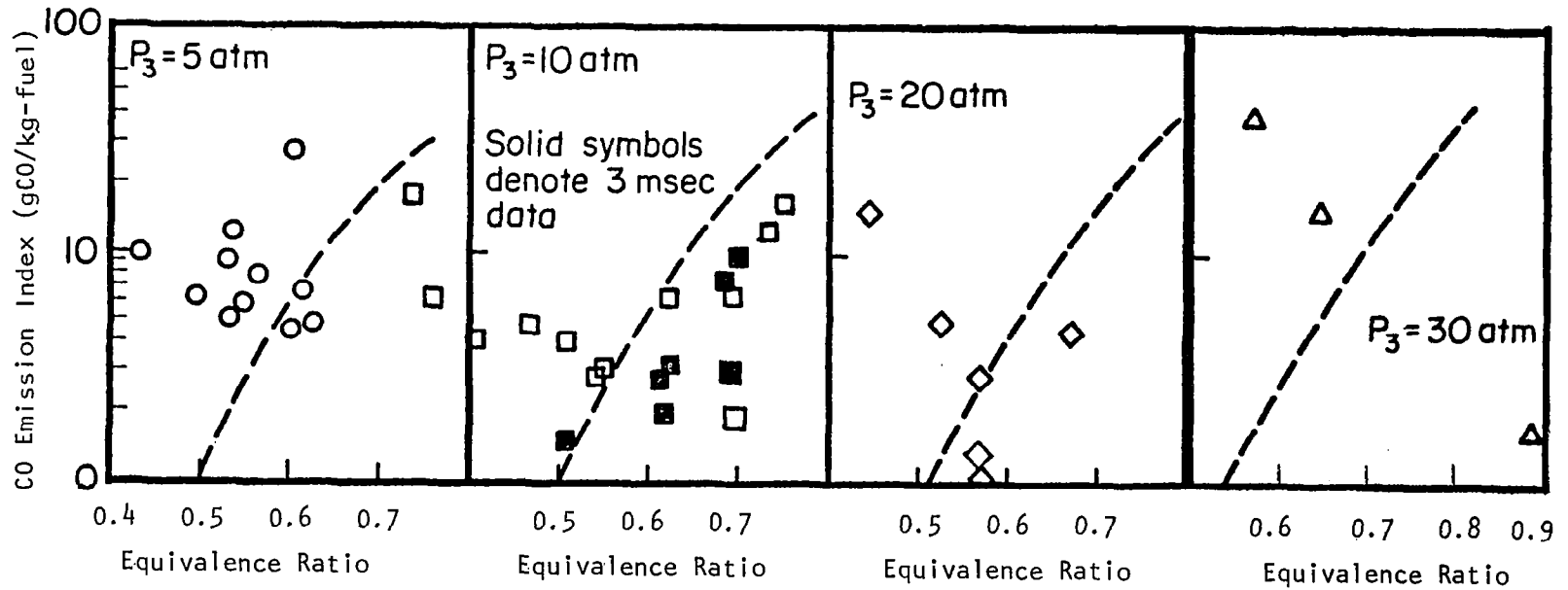


FIGURE 8b. CO EMISSION INDEX FOR 2 MSEC COMBUSTOR RESIDENCE TIME ( $T_3=800\text{K}$ )

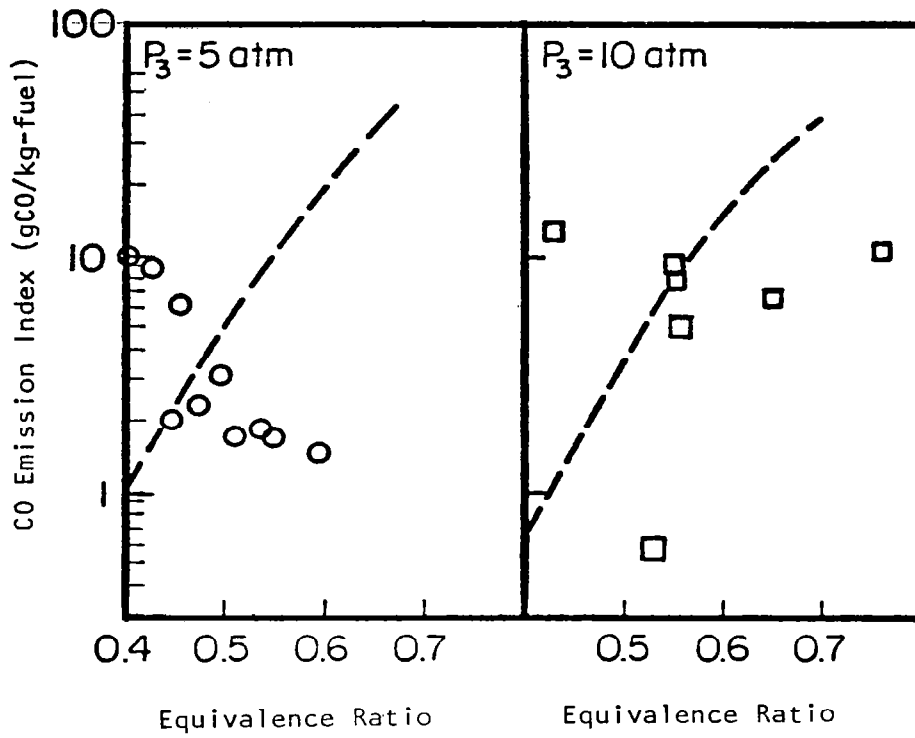


FIGURE 8c. CO EMISSION INDEX FOR 2 MSEC COMBUSTOR RESIDENCE TIME ( $T_3=1000\text{K}$ )

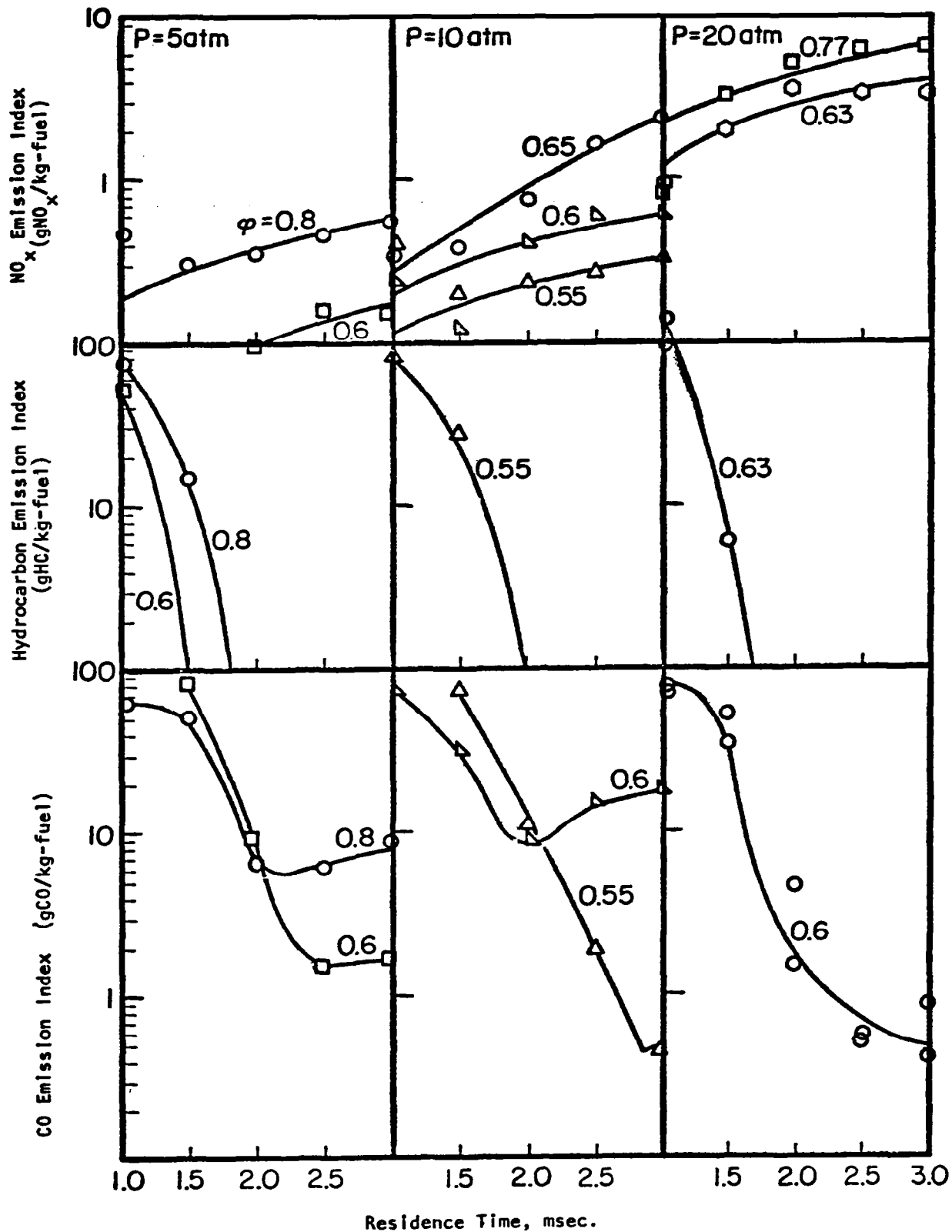


FIGURE 9a. EMISSION INDICES AS A FUNCTION OF COMBUSTOR RESIDENCE TIME ( $T_3=600\text{K}$ )



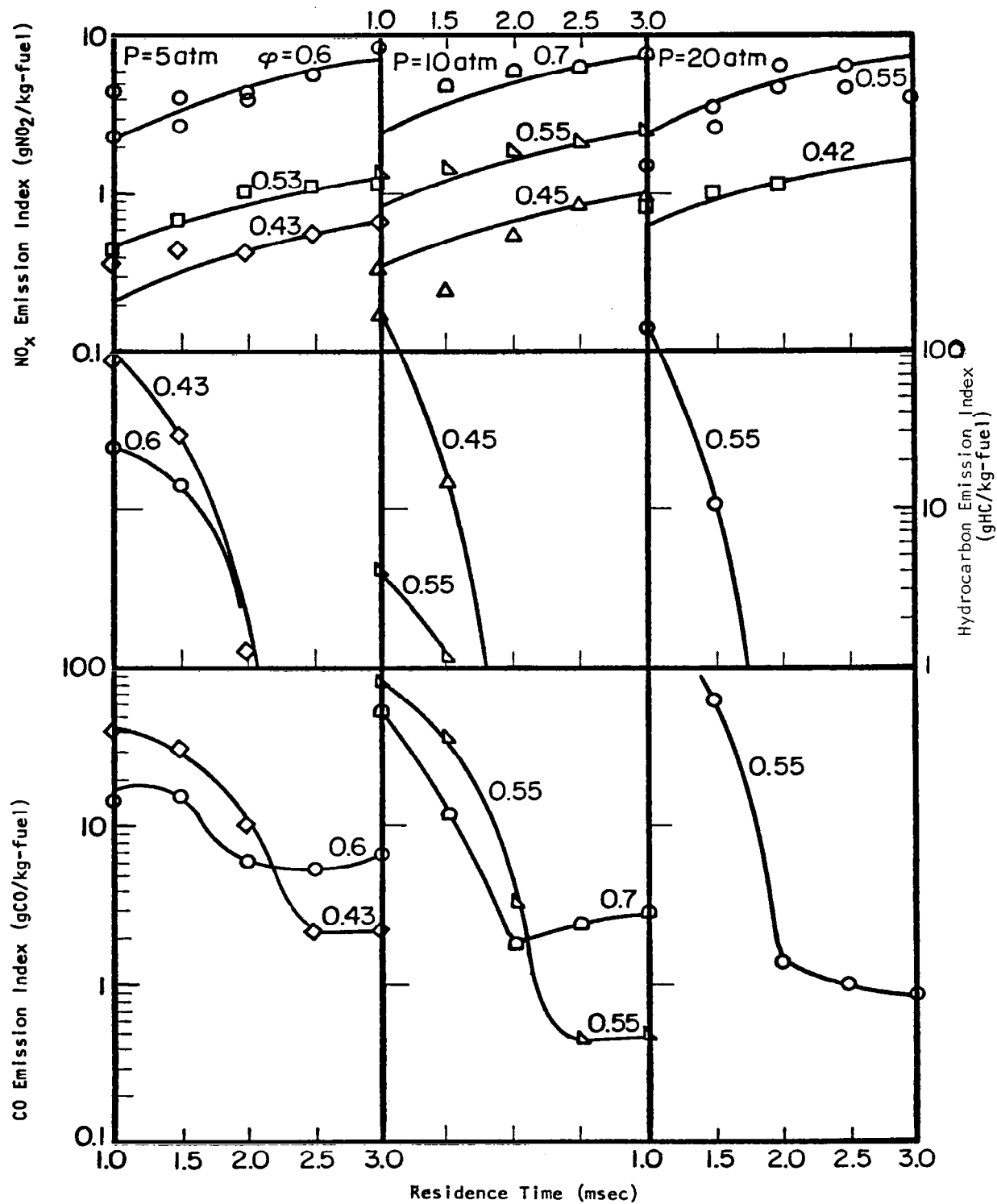


FIGURE 9b. EMISSION INDICES AS A FUNCTION OF COMBUSTOR RESIDENCE TIME ( $T_3=800K$ )

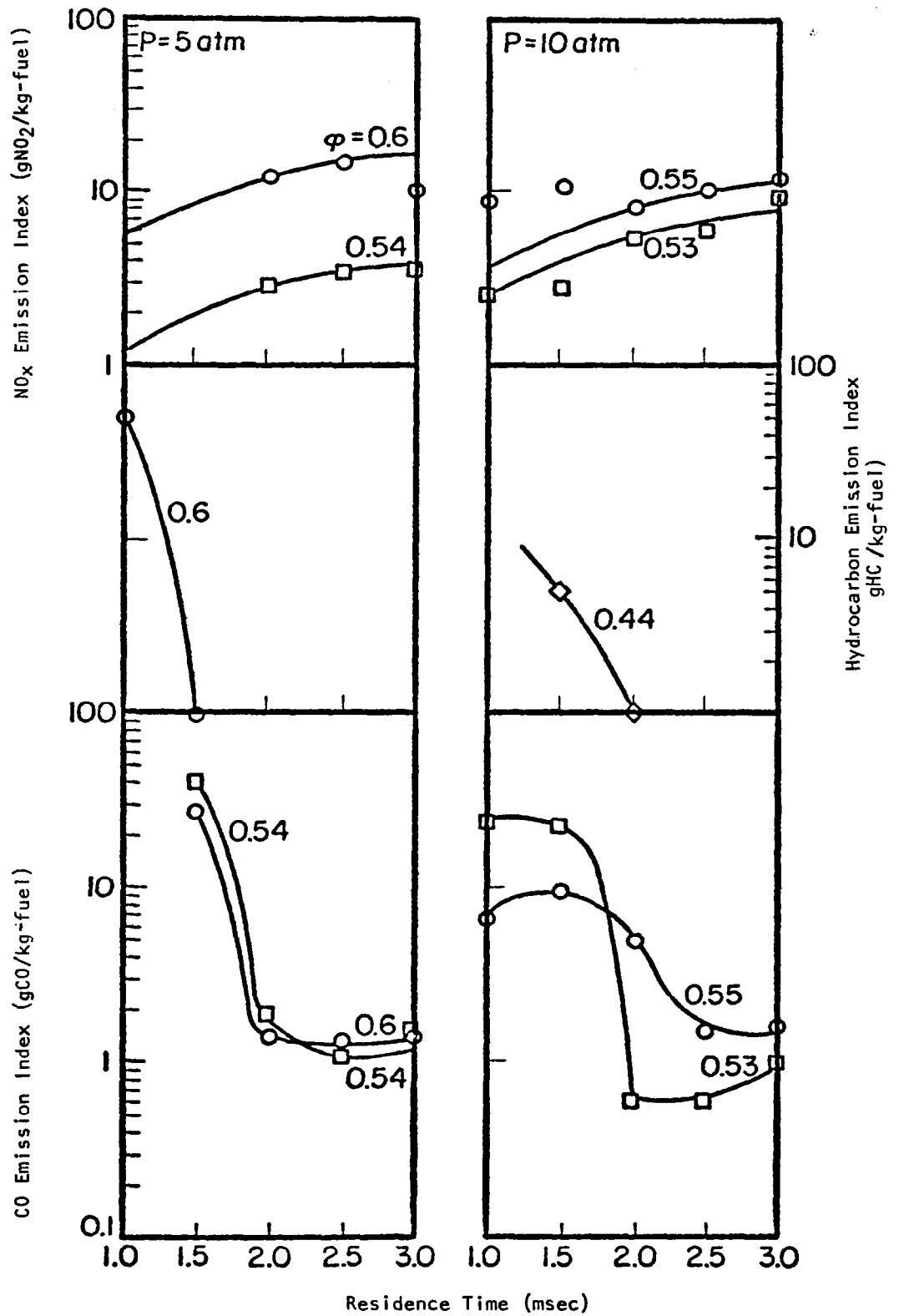


FIGURE 9c. EMISSION INDICES AS A FUNCTION OF COMBUSTOR RESIDENCE TIME ( $T_3=1000\text{K}$ )

## DISCUSSION

### Oxides of Nitrogen

The  $\text{NO}_x$  emissions measurements for a fixed combustor residence time of two milliseconds which were summarized in Figure (7) indicate that emission index is a strong function of both equivalence ratio and combustor entrance temperature. However, as  $\text{NO}_x$  production is basically a post-flame reaction, one would expect reaction rates to be strongly influenced by the adiabatic flame temperature and this parameter, itself a function of inlet temperature and equivalence ratio, has been found useful in previous studies as a correlation parameter. Accordingly, the  $\text{NO}_x$  emission index has been replotted as a function of adiabatic flame temperature and the results presented in Figure (10). At a pressure of 20 atm, plotting the data as a function of adiabatic flame temperature causes it to collapse quite nicely, indicating that  $\text{NO}_x$  emission index is a principal function of this parameter. At 30 atm, there is not sufficient data to support the same conclusion as only two data points could be obtained at the 30 atm/600K operating point due to the unstable nature of the combustion at this condition. (As noted earlier, these data had to be obtained with the gas igniter in operation and some effect of the igniter may be present.) Nevertheless, the assumption that  $\text{NO}_x$  emission index is principally a function of adiabatic flame temperature is certainly not contradicted by the limited data available.

At pressures of 5 atm and 10 atm, the situation is quite different. Here a complete collapse of the data definitely fails to occur. The data for inlet temperatures of 800K and 1000K falls quite close to the 20 atm collapsed data band.

Figure (11) presents the same data, regrouped in terms of common inlet temperature. Here, the relationship between inlet temperature and sensitivity to pressure level becomes clearer. At the 1000K inlet condition, changing pressure from 5 atm to 10 atm produces no discernable effect. At 800K, the data widens into a band with increasing pressure appearing to decrease the sensitivity to adiabatic flame temperature somewhat. At 600K,  $\text{NO}_x$  levels at 20 atm and 30 atm fall within the data band observed at 800K. However, at pressure below 20 atm  $\text{NO}_x$  level drops off very rapidly with decreasing pressure.

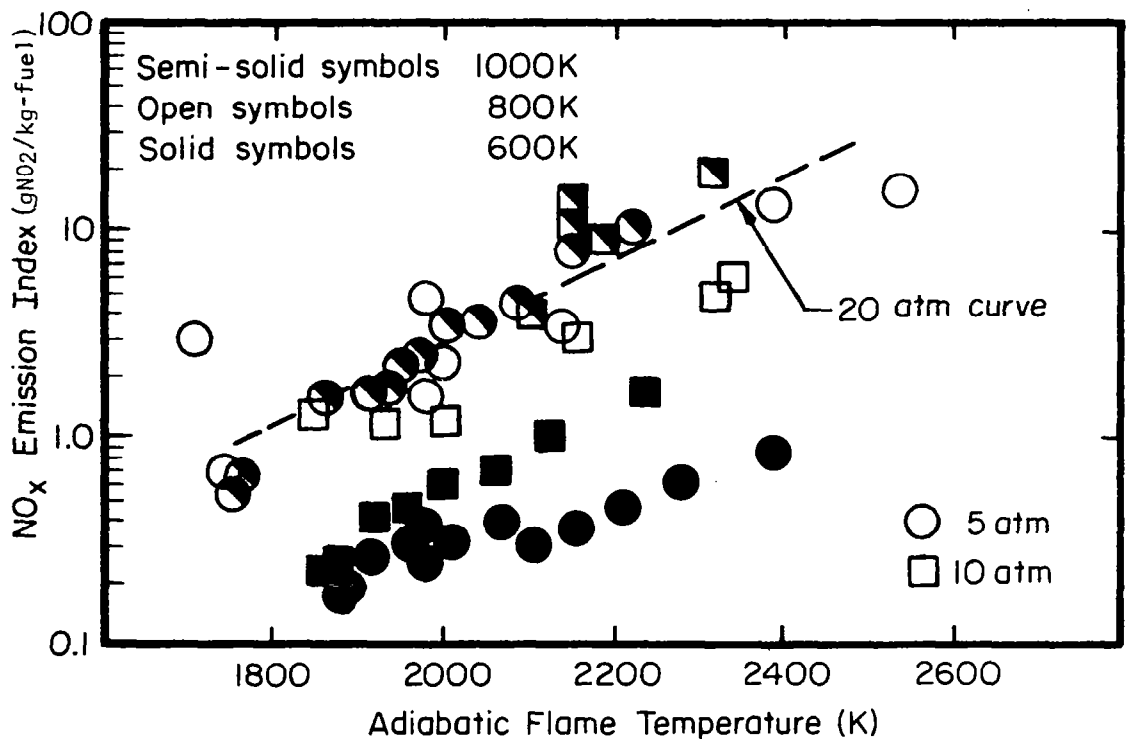
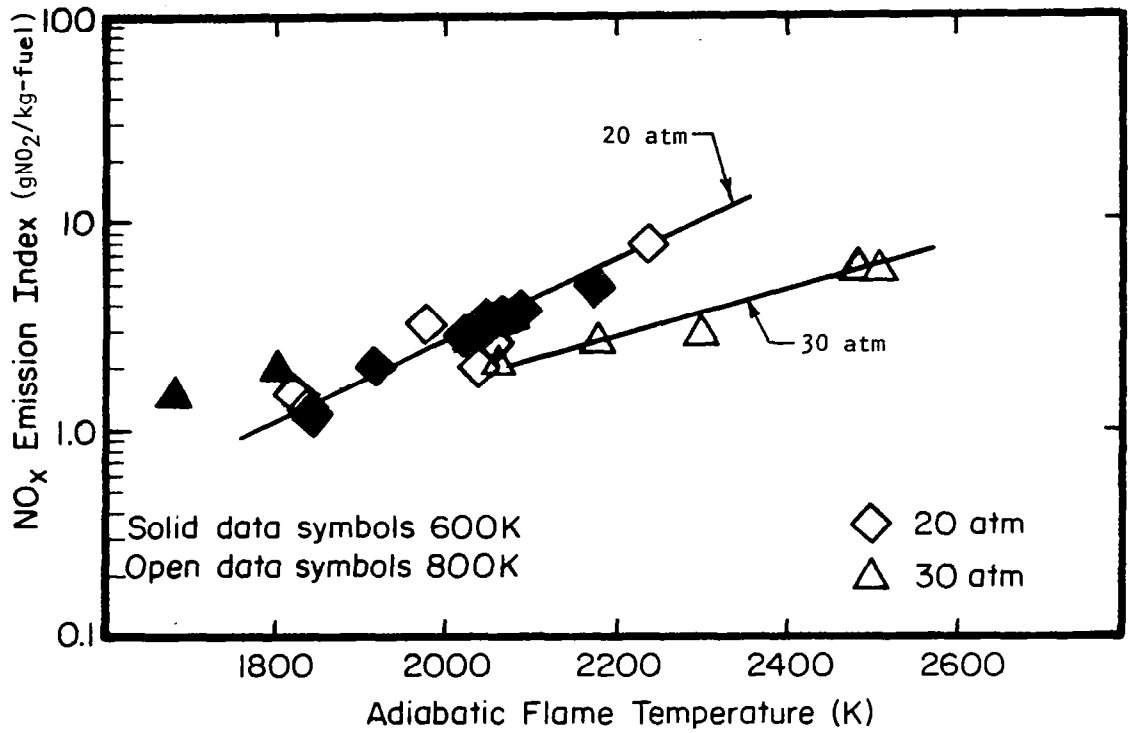


FIGURE 10. NO<sub>x</sub> EMISSION INDEX AS A FUNCTION OF ADIABATIC FLAME TEMPERATURE (RESIDENCE TIME 2 MSEC).

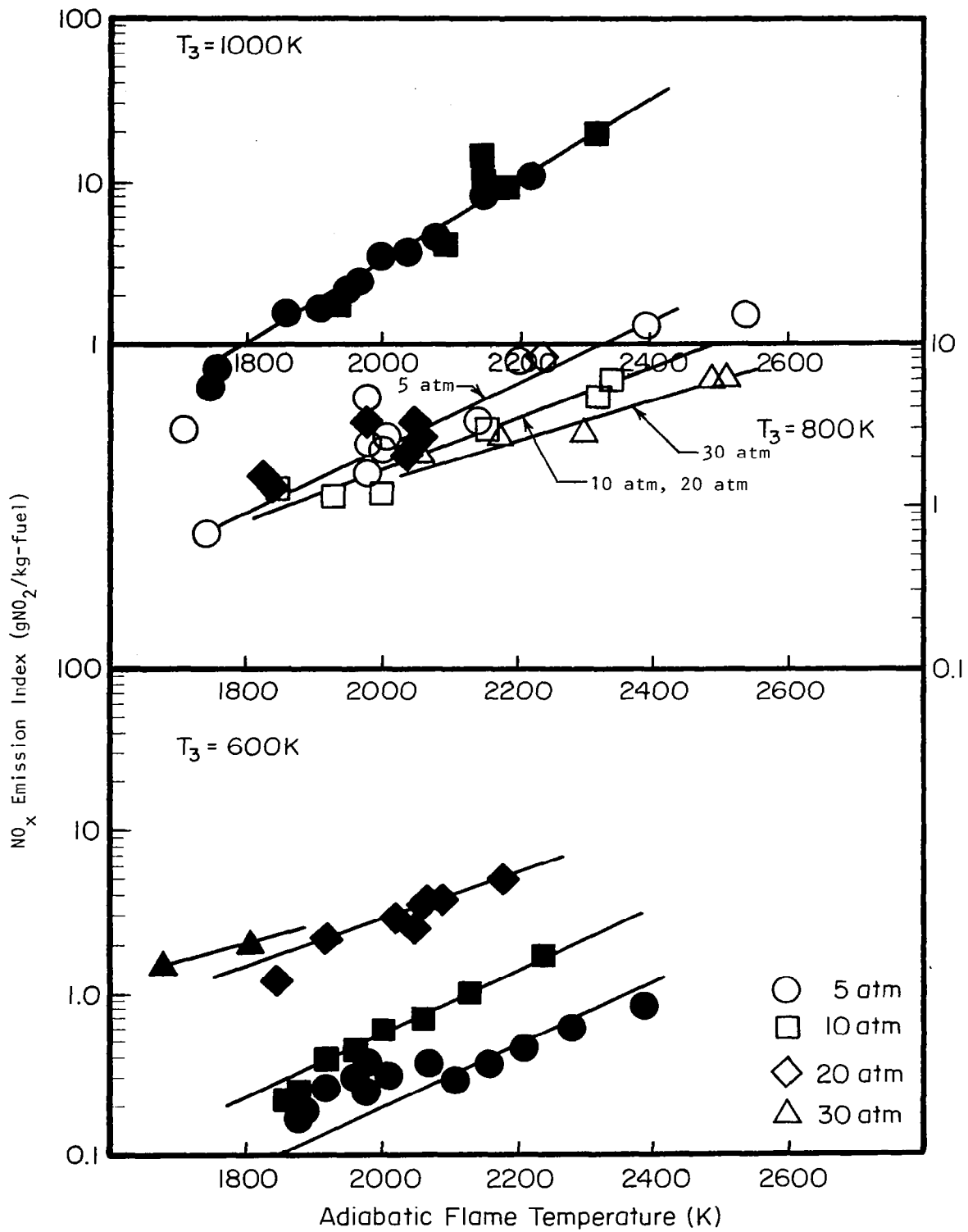


FIGURE 11.  $\text{NO}_x$  EMISSION INDEX AS A FUNCTION OF ADIABATIC FLAME TEMPERATURE (COMBUSTOR RESIDENCE TIME OF 2MSEC)

The  $\text{NO}_x$  emissions data are cross plotted in Figure (12) to illustrate the effect of pressure. The data for inlet temperatures of 1000K and 800K show a weak sensitivity to pressure. The 800K data is reasonably well represented by curves showing emission index to vary with the square root of pressure. The 30 atm/800K data does not fit well with the data obtained at lower pressures and it is possible that a similar phenomenon to that which resulted in unstable combustion at the 30 atm/600K point is at work here as well. For example, if the combustion region is not well anchored to the flameholder, the effective residence time may be smaller than two milliseconds.

$\text{NO}_x$  emissions data were presented in Figure (9) as functions of combustor residence time. The curves drawn through the data points represent a direct proportionality between emission index and residence time.  $\text{NO}_x$  levels measured at combustor stations corresponding to small values of residence time often fall above the linear rate curve, but these measurements probably reflect the incomplete mixing of local pockets of high  $\text{NO}_x$  produced in the longer residence time recirculation zones at the base of the flameholder. The linear increase of  $\text{NO}_x$  with combustor residence time indicates a post-flame reaction with no evidence of prompt  $\text{NO}_x$ , a finding in agreement with previous data for lean premixed systems. The linearity of the  $\text{NO}_x$  production curve is not dependent on equivalence ratio, pressure or combustor inlet temperature.

#### Unburned Hydrocarbons

Figure (9) shows a rapid disappearance of unburned hydrocarbon species with combustor residence time with levels becoming undetectable after 2 msec. In tests where emissions measurements were made as functions of equivalence ratio, inlet temperature and pressure for a fixed residence time of 2 msec, hydrocarbon species were generally below the limit of detection, even at equivalence ratios just above the lean stability limit.

#### Carbon Monoxide

Figure (9) indicated that carbon monoxide levels peak sometime between zero and one millisecond and then fall steadily until an equilibrium condition is attained. This behavior pattern does not appear to be strongly influenced by

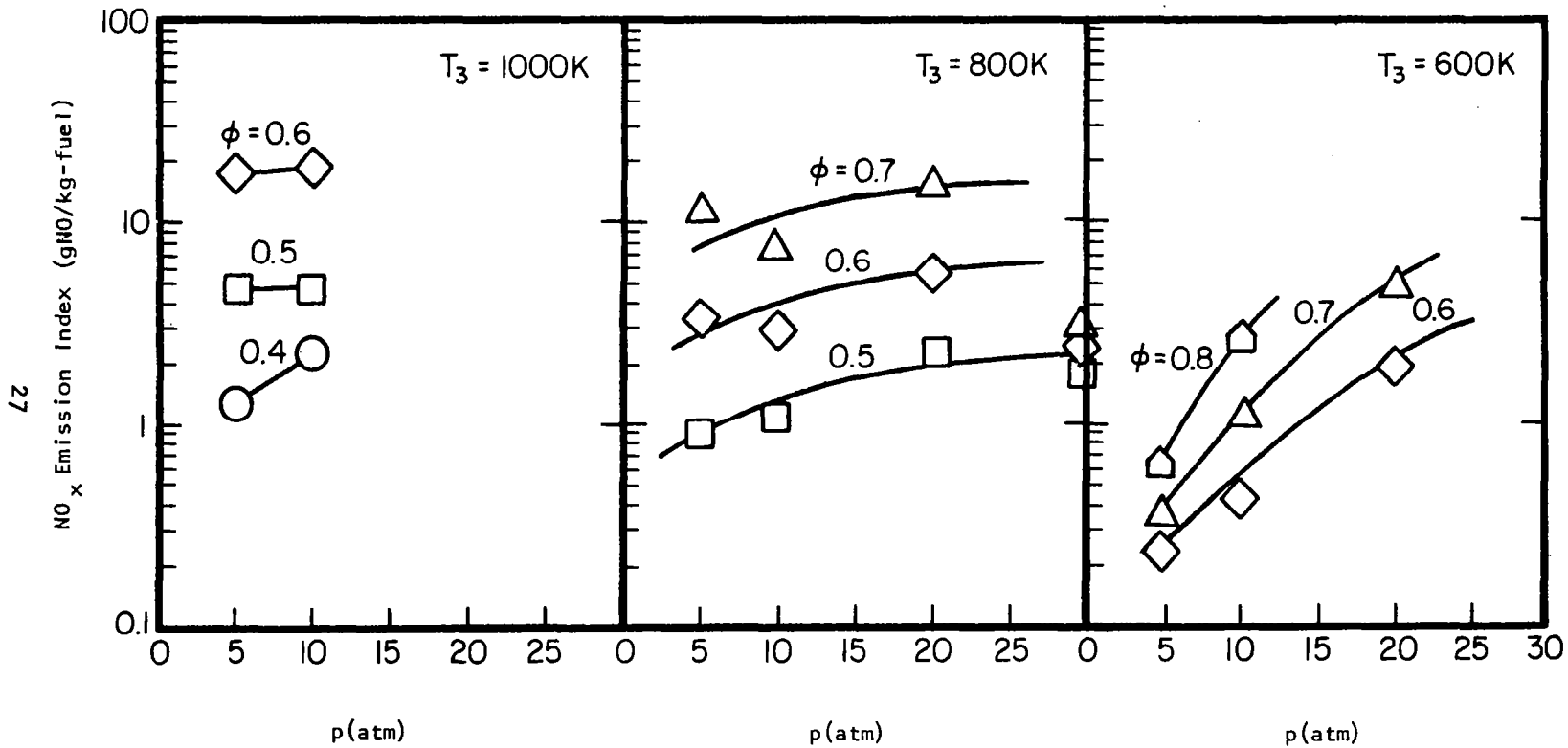


FIGURE 12. EFFECT OF PRESSURE ON  $\text{NO}_x$  EMISSION INDEX (COMBUSTOR RESIDENCE TIME 2 MSEC)

pressure, inlet temperature or equivalence ratio.

Figure (8) indicated that for any fixed value of inlet temperature and pressure, CO level drops steadily as equivalence ratio increases from the lean stability limit, reaches a minimum and then rises as equivalence ratio increases still further. This behavior is evident at all conditions tested but is probably most easily seen in the 10 atm-800K data. Qualitatively, one would normally expect the data to behave in this manner. However, from a quantitative viewpoint, one would also expect to see the CO level rising along the chemical equilibrium curve. The fact that measured CO levels are below equilibrium raises the possibility of an inadequate quenching rate in the sampling probe. In an effort to verify that an equilibrium condition had indeed been achieved after the CO curve reached its minimum, a scan of CO was made as a function of equivalence ratio for the 10 atm - 800K condition and a residence time of 3 milliseconds. The results of this scan, shown in Figure (8) by the solid symbols, indicate that no significant change in CO level takes place between the 2 msec and 3 msec positions. As a result, the mixture should be in chemical equilibrium and a loss of CO during the probe quenching process appears quite likely. It is difficult to estimate the magnitude of the error in CO level since the degree of reaction during the sample quenching process varies with the test condition.

Despite the apparent difficulty in obtaining an accurate CO sample, a close examination of the data yields an extremely interesting result. As a design criterion, one is interested in the CO breakpoint, that is, the point at which CO levels break away from the equilibrium curve. Equivalence ratios above the breakpoint will produce equilibrium CO concentrations; from the point of view of combustion efficiency, equilibrium represents an optimum condition with regard to CO. Defining the breakpoint as the point at which measured CO level crosses the equilibrium curve, Figure (8) yields a series of breakpoint equivalence ratios depending upon the inlet temperature and pressure. However, when the adiabatic flame temperature corresponding to the observed breakpoints is calculated, one obtains the interesting result, illustrated in Figure (13), that breakpoint adiabatic flame temperature is essentially constant and equal to 2050K.



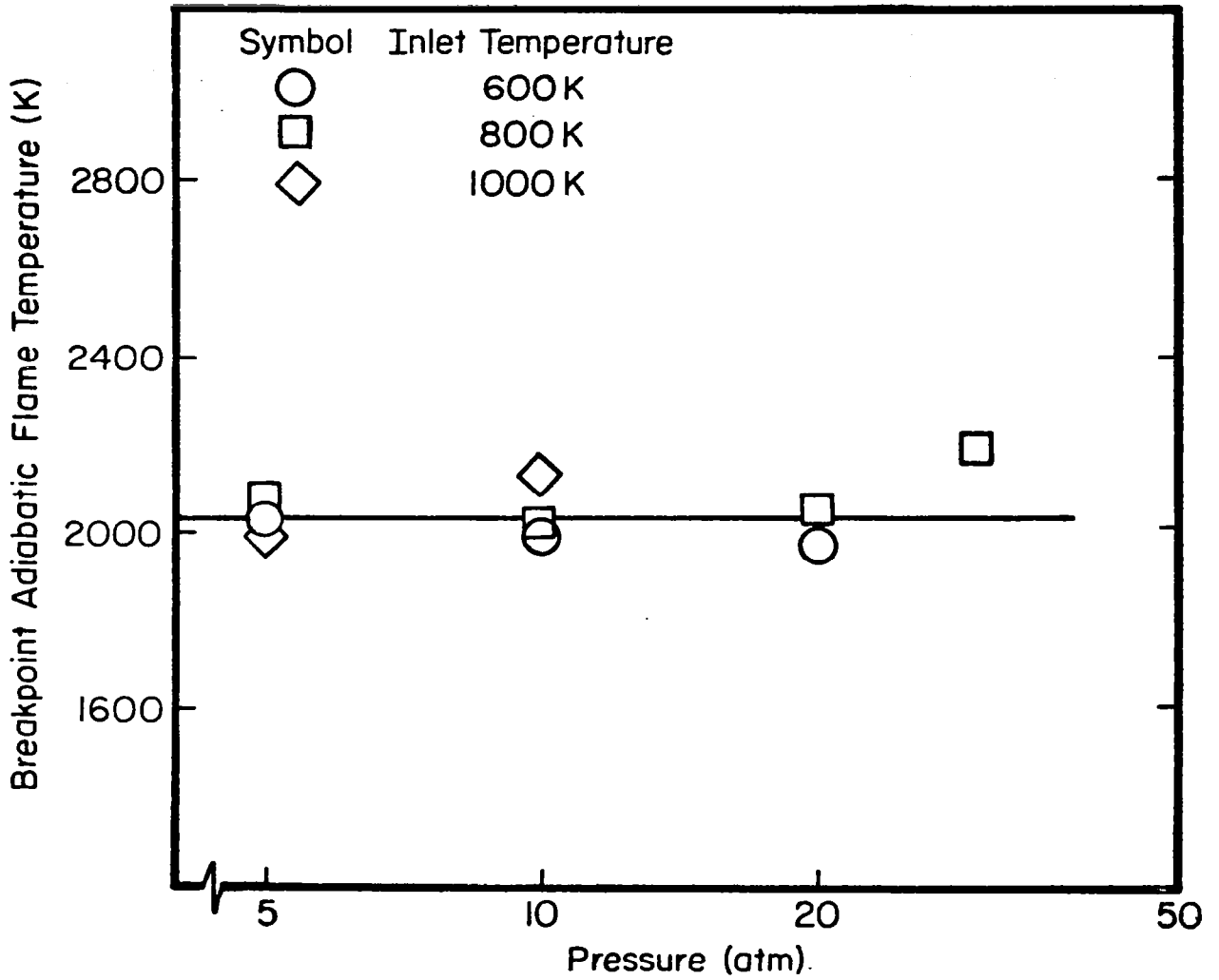


FIGURE 13. ADIABATIC FLAME TEMPERATURE CORRESPONDING TO CO BREAKPOINT AT 2 MSEC RESIDENCE TIME.

## Combustion Inefficiency

Combustion inefficiency, defined in Appendix A, is calculated from a properly weighted sum of unburned hydrocarbon emissions and the excess of CO above that corresponding to chemical equilibrium. Since unburned hydrocarbon levels are negligible after 2 msec residence time and CO reaches an equilibrium condition after 2.5 msec, the condition of less than 0.01% combustion inefficiency is attained for residence times of 2.5 msec or more and adiabatic flame temperatures greater than or equal to 2050K.

For a fixed residence time of 2 msec, combustion inefficiency can be calculated from the CO and unburned hydrocarbon data for the variety of conditions tested. The results of this calculation are presented in Figure (14), where combustion inefficiency at 2 msec residence time is shown as a function of equivalence ratio for each of the pressure-inlet temperature conditions in the test matrix. A particularly significant point is that, with the exception of one data point, combustion inefficiency never exceeded 1%.

## Lean Stability Limit

The lean stability limit was measured by establishing a flame at a given equivalence ratio, pressure and inlet temperature and gradually lowering the equivalence ratio until the flame blew out. Over the range of parameters covered in this program, the lean stability limit was found to correspond to an adiabatic flame temperature of approximately 1800K with a small perturbation produced by inlet temperature. More precisely,

$$T_{4_{LSL}} \text{ (K)} = 1800 + 0.25(800 - T_3)$$

The second term in the expression for the lean stability limit adiabatic flame temperature ( $T_{4_{LSL}}$ ) is relatively small, representing a perturbation of  $\pm 50K$  over the range of inlet temperatures tested. Increasing pressure does not affect the lean stability limit.

## Operational Observations

The design of the flameholder and the transient operating characteristics of

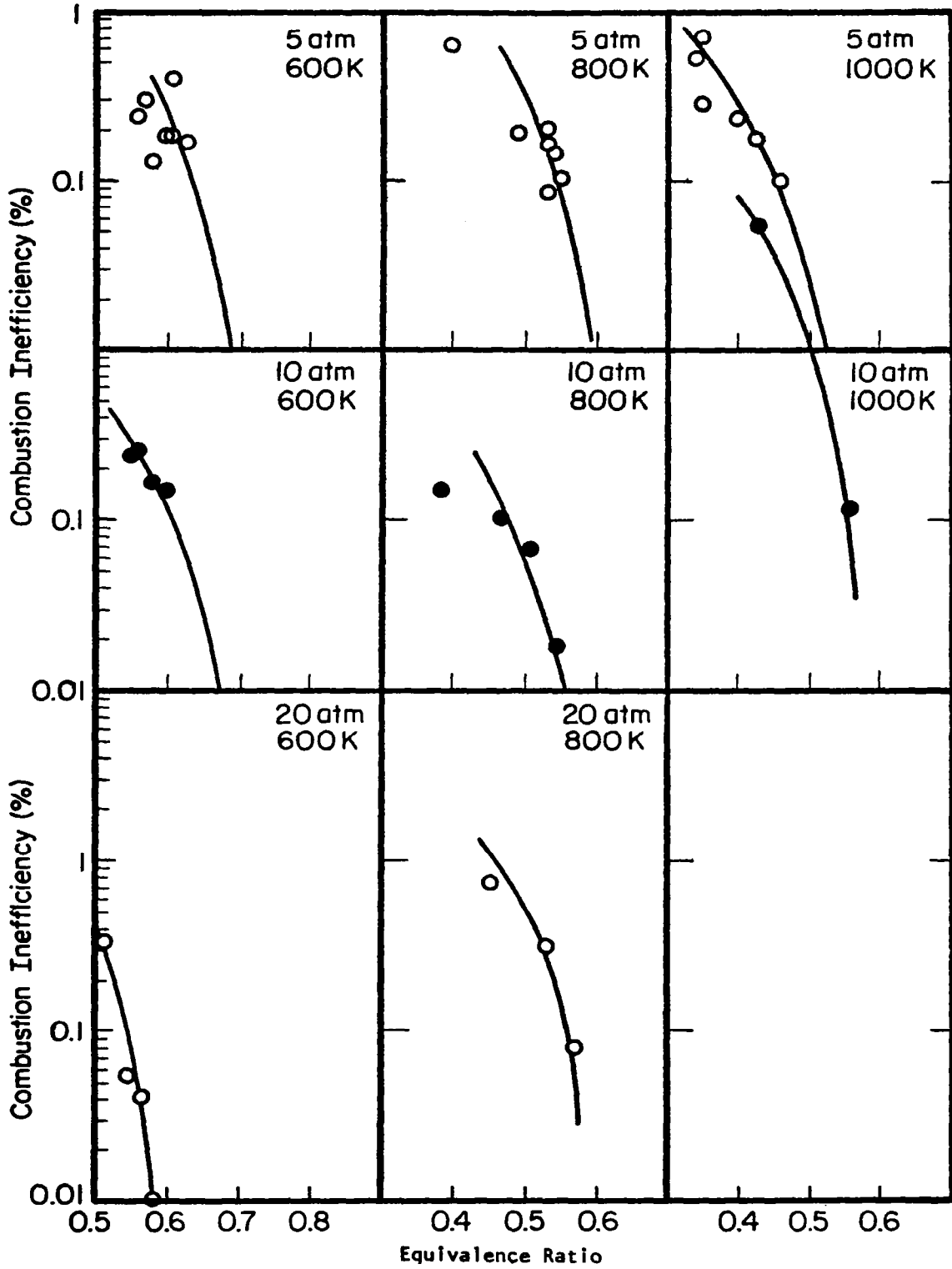


FIGURE 14. COMBUSTION INEFFICIENCY AS A FUNCTION OF EQUIVALENCE RATIO

the test apparatus appear to have a pronounced influence on the ability to operate without encountering flashback. For a given flameholder geometry very rapid changes in pressure (such as those which could be produced by a sudden increase in equivalence ratio) were found to cause the flame to move upstream into the mixer. This problem would appear to be associated with the very low dynamic pressure of the gas streams in the passages through the flameholder, varying from 2½% to 4% of the static pressure level, depending on inlet temperature. As a result, a transient static pressure increase in the combustor in excess of 4% can cause a temporary flow reversal, allowing chemically and thermally active gas from the combustor to travel upstream.

In addition to transient phenomena, the details of the flameholder design appear to have an important bearing on the flashback problem. Initial attempts to light the burner at the 800K - 20 atm condition consistently produced flashback. However, when the radius at the entrance to the flameholder perforations was increased from 1mm to 3mm, ignition at 800K - 20 atm no longer produced flashback. The modified design was still subject to flashback at the next higher temperature (1000K - 20 atm) condition but wall thickness limitations prevented increasing the entrance radius still further.

It is of interest to note that early testing employed a slightly different flameholder than that described in Section II. The original flameholder design employed a larger number of perforations each with a diameter 2/3 that eventually employed (same overall blockage) and made no attempt to round the entrance corners other than the slight natural rounding provided by weld beads. Occasionally, apparently depending upon operating transients, this flameholder would suffer flame damage in some, but not all, of the passages. Increasing the passage diameter, at constant blockage, and providing a small radius at the entrance eliminated this problem.

In light of this experience, it appears possible that the sudden contraction produced at the entrance to the passages of the perforated plate results in a small region of locally separated flow. The gas in this region may be ignited by the upstream convection of hot gas during a pressure transient, by conditions of high pressure/temperature which reduce ignition delay time or a combination of these effects. Clearly, the flashback phenomenon and its relationship to flameholder geometry bears further investigation.

## SUMMARY OF RESULTS

1. At inlet temperatures of 800K and 1000K, the  $\text{NO}_x$  emissions of a premixed propane/air flame display only moderate sensitivity to pressure.  $\text{NO}_x$  emission data taken at an inlet temperature of 800K is reasonably well fit by curves of the form  $E_{\text{NO}_x} \sim \sqrt{P}$ . At an inlet temperature of 600K, observed  $\text{NO}_x$  levels dropped markedly with decreasing pressure for pressures below 20 atm.
2.  $\text{NO}_x$  levels are directly proportional to combustor residence time and formation rates are principally a function of adiabatic flame temperature.
3. CO levels peak sometime during the first millisecond of combustor residence time and then decrease until an equilibrium condition is attained. For adiabatic flame temperatures of 2050K and higher, CO reaches chemical equilibrium within 2 msec.
4. Unburned hydrocarbon species drop to a negligible level within 2 msec regardless of inlet temperature, pressure or equivalence ratio. Increasing adiabatic flame temperature increases the destruction rate of UHC species.
5. For a combustor residence time of 2.5 msec, combustion inefficiency becomes less than 0.01% at an adiabatic flame temperature of 2050K. The maximum combustion inefficiency observed for a 2.0 msec residence time was on the order of 1% and correspond to conditions near the lean stability limit.
6. When using a perforated plate flameholder, the lean stability limit is well represented by the condition of 1800K adiabatic flame temperature. There is a small effect of inlet temperature with  $\pm 200\text{K}$  excursions in this variable causing the stability limit to vary by  $\pm 50\text{K}$ .

APPENDIX A  
DATA REDUCTION PROCEDURES

The gas analysis instrumentation provide rawdata in the form of volume fractions of the particular gases being sampled. This raw data is converted into the more convenient form of emission index and equivalence ratio following the procedures detailed below.

Each of the gas analysis instruments must be calibrated in order to convert the instrument reading to the volume fraction of the particular gas being analyzed. In the case of the Beckman Model 402 hydrocarbon analyzer and the Beckman Model 315B CO analyzer, this calibration is accomplished by passing prepared mixtures of calibration gas through the instruments and establishing calibration curves. The hydrocarbon analyzer was calibrated using gas standards containing 982 ppm and 99 ppm propane in nitrogen. The instrument output is proportional to the number of carbon atoms with hydrogen bonds. Thus, pure hydrogen or pure carbon will produce no response and a given concentration of propane ( $C_3H_8$ ) will produce three times the response of an equal concentration of methane ( $CH_4$ ). The instrument responds to all C-H bonds. As a result, it measures the sum of both unoxidized hydrocarbon and partially oxidized hydrocarbon molecules. The instrument calibration curve is shown in Figure (A1). The response is linear with hydrocarbon concentration, presented in units of ppmC, that is, the number of hydrogenated carbon atoms in parts per million.

Calibration of the Beckman Model 315B CO analyzer was accomplished using standard gases with 2530 ppm, 1530 ppm, 916 ppm, 608 ppm, 305 ppm and 64 ppm CO in nitrogen. The calibration curve is shown in Figure (A1).

The gases used for calibration of the Beckman Model 864  $CO_2$  analyzer contained 15.3%, 10.0%, 5.0% and 2.0%  $CO_2$  in nitrogen. The analyzer calibration curve is slightly nonlinear as shown in Figure (A1). The Beckman Model 951  $NO/NO_x$  analyzer was calibrated using standards containing 411 ppm, 197 ppm, 91 ppm and 52 ppm  $NO_x$  in nitrogen. The  $NO_x$  analyzer produces a linear response up to 140 ppm as illustrated in Figure (A1).

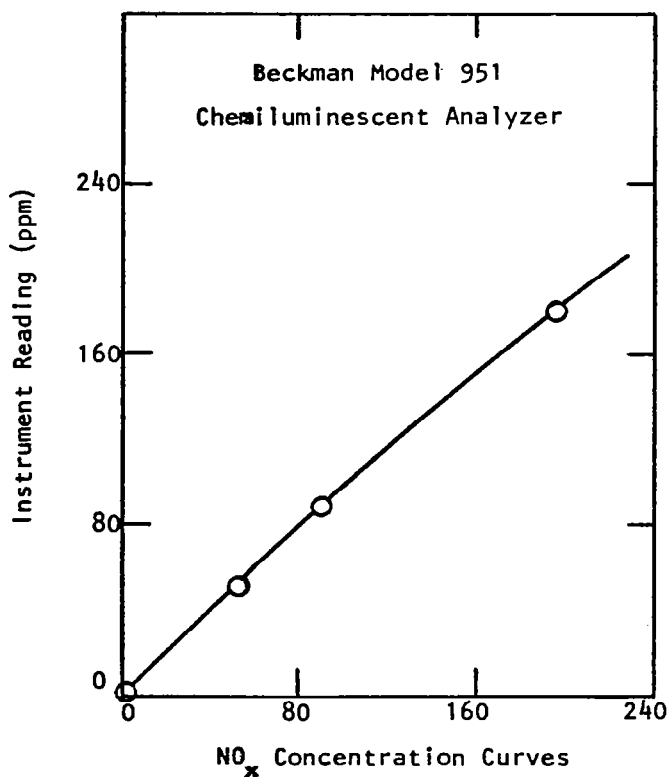
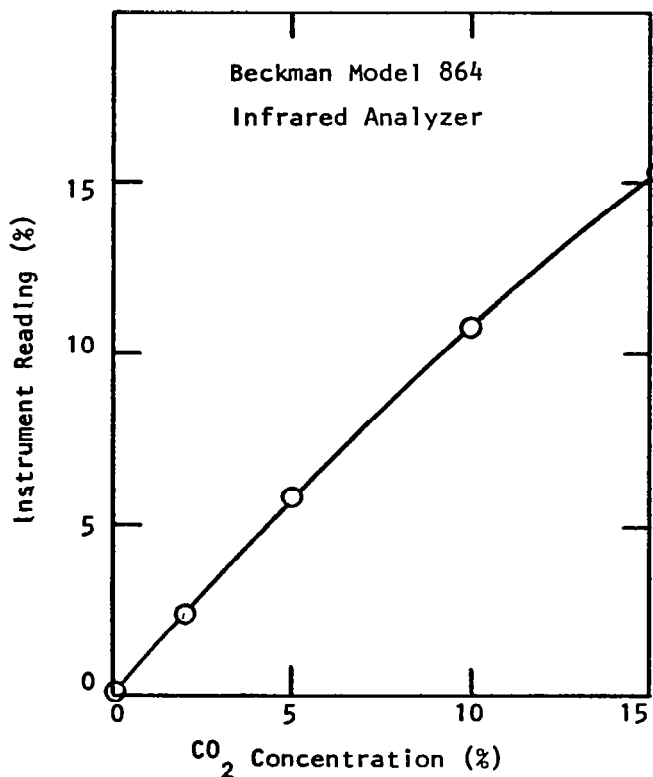
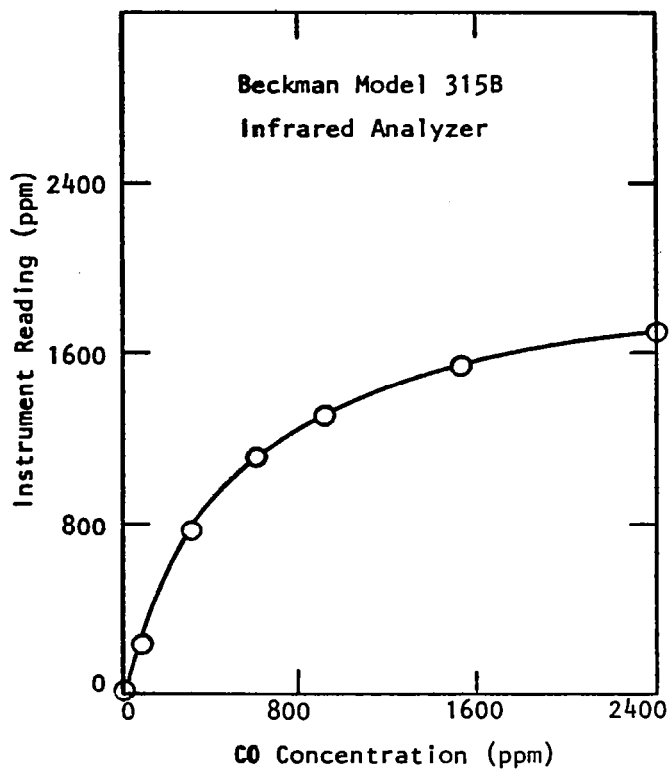
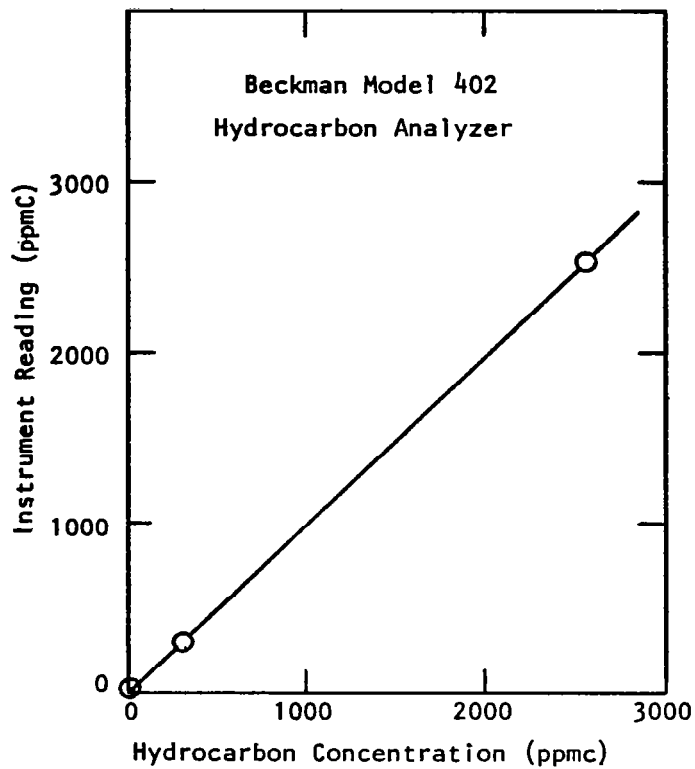


FIGURE A1. GAS ANALYSIS INSTRUMENT CALIBRATION CURVES

The gas analysis instruments were calibrated once each week using the entire set of standard gases. Zero gas and span gas were passed through all instruments immediately prior to each test and instrument output recorded on the same data roll which was used for the subsequent test run.

Conversion of the molar concentration (volume fractions) provided by the gas analysis instrumentation into the more convenient terms of emission index and equivalence ratio requires a prior knowledge of the ratio of carbon to hydrogen in the system. This is ascertained from a chemical analysis of the fuel used in the experiments. For propane, the hydrogen to carbon ratio is 2.667 and the fuel/air ratio  $f/a$  is given by

$$f/a = \frac{CO \times 10^{-4} + CO_2 + HC \times 10^{-4}}{198 - 2.3 \times 10^{-4} CO - 1.32 CO_2} \quad (A1)$$

where CO and HC are the molar concentrations of carbon monoxide and unburned hydrocarbon in units of parts per million (ppm) and ppmC respectively and  $CO_2$  is the volume percent of carbon dioxide expressed as a percentage of total gas volume.

The equivalence ratio,  $\phi$ , is defined as the ratio of the actual fuel/air ratio to the stoichiometric fuel/air ratio. For propane,

$$\phi = 15.8 (f/a) \quad (A2)$$

The combustion inefficiency, CI, is

$$CI = \frac{0.426 CO + 1.019 HC}{10^4 CO_2 + CO + HC} \times 100$$

The numerator of the second term represents the potential heat release which could be obtained by further oxidation of CO to form  $CO_2$  and hydrocarbons to form  $H_2O$  and  $CO_2$ . However, a certain level of CO is required by chemical equilibrium considerations. Since the production of the equilibrium CO level



does not imply combustor inefficiency, the definition of percent combustion inefficiency CI is altered slightly so that a penalty accrues only from that portion of the total CO produced which exceeds the equilibrium value. Thus,

$$CI = \frac{0.426 (CO - CO_{eq}) + 1.019 HC}{10^{+4} CO_2 + CO + HC} \quad (A3)$$

The measured volume fractions expressed as ppm of CO, hydrocarbons and NO<sub>x</sub> are converted into emission indices (grams of component per kilogram of fuel) using the following expressions:

$$E_{CO} = \frac{CO (1 + f/a)}{1034 f/a} \quad (A4)$$

$$E_{HC} = \frac{HC (1 + f/a)}{2069 f/a} \quad (A5)$$

$$E_{NO_x} = \frac{NO_x (1 + f/a)}{630 f/a} \quad (A6)$$

APPENDIX B  
DATA SUMMARY

$P_3$	$T_3$	$\tau_R$	$\phi$	$NO_x$	UHC	CO	$E_{NO_x}$	$E_{HC}$	$E_{CO}$	CI
(atm)	(K)	(msec)		(ppm)	(ppmC)	(ppm)	(g/kg)	(g/kg)	(g/kg)	(%)
5	600	3.0	0.78	16.8	58	420	0.562	0.594	8.56	
5	600	3.0	0.61	3.2	52	65	0.137	0.673	1.68	
5	600	2.5	0.78	14.1	38	300	0.471	0.382	6.12	
5	600	2.5	0.61	3.4	50	60	0.146	0.647	1.55	
5	600	2.0	0.78	11.1	27	325	0.370	0.276	6.63	
5	600	2.0	0.61	2.2	10	345	0.094	0.135	8.93	
5	600	2.0	0.74	12.8	2520	340	0.451	28.4	7.27	
5	600	2.0	0.66	5.6	410	170	0.377	5.15	4.06	
5	600	2.0	0.58	6.2	37	182	0.279	0.534	4.92	0.12
5	600	2.0	0.56	4.0	38	330	0.187	0.553	9.24	0.23
5	600	2.0	0.57	4.2	75	340	0.194	1.10	9.44	0.24
5	600	2.0	0.57	2.2	10	345	0.100	0.15	9.45	
5	600	2.0	0.63	7.65	71	280	0.319	0.942	7.06	0.17
5	600	2.0	0.61	9.35	3892	300	0.401	53.2	7.79	0.19
5	600	2.0	0.60	7.06	2233	220	0.306	30.8	7.87	0.19
5	600	2.0	0.61	5.77	205	320	0.246	2.79	8.27	0.19
5	600	2.0	0.67	7.35	82	600	0.286	1.02	14.1	
5	600	2.0	0.71	9.35	656	480	0.345	7.7	10.7	
5	600	2.0	0.78	15.3	102	580	0.52	1.11	11.9	
5	600	2.0	0.86	26.2	0	1000	0.807	0	18.6	
5	600	1.5	0.78	8.72	1434	2530	0.292	14.6	51.6	

APPENDIX B  
DATA SUMMARY

$P_3$	$T_3$	$\tau_R$	$\phi$	$NO_x$	UHC	CO	$E_{NO_x}$	$E_{HC}$	$E_{CO}$	CI
(atm)	(K)	(msec)		(ppm)	(ppmC)	(ppm)	(g/kg)	(g/kg)	(g/kg)	(%)
5	600	1.5	0.61	7.94	62.5	>3000	0.337	0.808	>80	
5	600	1.0	0.78	12.95	7416	>3000	0.433	75.6	>60	
5	600	1.0	0.61	15	4056	>3000	0.637	52.5	>80	
10	600	3.0	0.55	7.1	0	16	0.33	0	0.45	
10	600	3.0	0.65	62.5	N.R	54	2.48		1.3	
10	600	3.0	0.61	13.2	0	670	0.554	0	17.1	
10	600	3.0	0.92	75	0		2.14	0		
10	600	2.5	0.55	6	0	64	0.28	0	1.8	
10	600	2.5	0.65	44.5		54	1.77		1.3	
10	600	2.5	0.61	13.3	0	630	0.558	0	16.1	
10	600	2.5	0.92	27	0		0.87	0		
10	600	2.0	0.61	9.9	0	320	0.415	0	8.2	0.160
10	600	2.0	0.76	53	0	43	1.82	0	0.9	
10	600	2.0	0.69	27.7	0	35	1.03	0	0.8	
10	600	2.0	0.62	15.1	0	34	0.623	0	0.79	
10	600	2.0	0.60	10.7	0	35	0.461	0	0.79	
10	600	2.0	0.56	5.8	0	450	0.26	0	12.5	0.257
10	600	2.0	0.55	4.9	0	385	0.23	0	10.9	0.232
10	600	2.0	0.65	18.9		54	0.75		1.3	
10	600	2.0	0.92	21.8	0		0.7	0		
10	600	1.5	0.55	4.14	2025	2640	0.19	28.6	75	

APPENDIX B  
DATA SUMMARY

$P_3$	$T_3$	$\tau_R$	$\phi$	$NO_x$	UHC	CO	$E_{NO_x}$	$E_{HC}$	$E_{CO}$	CI
(atm)	(K)	(msec)		(ppm)	(ppmC)	(ppm)	(g/kg)	(g/kg)	(g/kg)	(%)
10	600	1.5	0.65	9.5		54	0.38		1.3	
10	600	1.5	0.61	2.8	1160	1260	0.12	14.8	32.2	
10	600	1.5	0.92	4.9	550		0.16	5.4		
10	600	1.0	0.61	6.4	6300	>3000	0.27	80	>80	
10	600	1.0	0.55	8.8	6214	3180	0.41	88	>90	
10	600	1.0	0.65	9.5		54	0.38		1.3	
10	600	1.0	0.92	6.4	3108		0.21	30.5		
20	600	3.0	0.58		20.8	15		0.279	0.402	
20	600	3.0	0.62		41.6	35		0.527	0.888	
20	600	3.0	0.77	189	0	35	6.42	0	0.721	
20	600	3.0	0.63	81.5	0	4	3.35	0	0.1	
20	600	2.5	0.58		18.7	20		0.251	0.537	
20	600	2.5	0.62		16.6	20		0.210	0.507	
20	600	2.5	0.80	197	0	45	6.67	0	0.927	
20	600	2.5	0.63	81.1	0	4	3.39	0	0.1	
20	600	2.0	0.66	87		45	3.47		1.09	
20	600	2.0	0.66	95		40	3.77		0.962	
20	600	2.0	0.72	142		50	5.18		1.10	
20	600	2.0	0.67	90.5		55	3.55		1.31	
20	600	2.0	0.65	64.5		55	2.60		1.34	
20	600	2.0	0.63	72.6		56	3.00		1.40	

40

APPENDIX B  
DATA SUMMARY

$P_3$	$T_3$	$\tau_R$	$\phi$	$NO_x$	UHC	CO	$E_{NO_x}$	$E_{HC}$	$E_{CO}$	CI
(atm)	(K)	(msec)		(ppm)	(ppmC)	(ppm)	(g/kg)	(g/kg)	(g/kg)	(%)
20	600	2.0	0.58	48.5		50	2.17		1.36	0.011
20	600	2.0	0.55	25.5		100	1.21		2.87	0.054
20	600	2.0	0.58		20.8	175		0.279	4.70	
20	600	2.0	0.62		14.5	55		0.184	1.40	
20	600	2.0	0.66		31.2	60		0.397	1.45	
20	600	2.0	0.65		20.8	100		0.266	2.43	
20	600	2.0	0.56		12.5	160		0.183	4.46	0.04
20	600	2.0	0.51		39.5	400		0.63	12.2	0.329
20	600	2.0	0.77	159.1	0	52	5.38	0	1.07	
20	600	2.0	0.63	90.5	0	5	3.72	0	0.125	
20	600	1.5	0.58		463	2000		6.21	53.7	
20	600	1.5	0.62		201	1350		2.55	34.2	
20	600	1.5	0.77	99.3	7.2	120	3.36	0.074	2.47	
20	600	1.5	0.63	48.4	98.8	680	1.99	1.24	17.0	
20	600	1.0	0.58		10660	>3000		142	>80	
20	600	1.0	0.62		7500	>3000		95.1	>75	
20	600	1.0	0.77	25.0	5473	1000	0.846	56.4	20.6	
20	600	1.0	0.63	22.2	11800	>3000	0.913	147	>75	
5	800	3.0	0.54	78.7	0	80	3.64	0	2.3	
5	800	3.0	0.43	11.5	0	0.677	0.56	0	2.15	
5	800	3.0	0.82	325	0	200	10.3	0	3.88	

14

APPENDIX B  
DATA SUMMARY

$P_3$	$T_3$	$\tau_R$	$\phi$	$NO_x$	UHC	CO	$E_{NO_x}$	$E_{HC}$	$E_{CO}$	GI
(atm)	(K)	(msec)		(ppm)	(ppmC)	(ppm)	(g/kg)	(g/kg)	(g/kg)	(%)
5	800	3.0	0.61	200	0	160	8.4	0	6.7	
5	800	2.5	0.54	77	0	90	3.56	0	2.62	
5	800	2.5	0.43	9.5	0	60	0.56	0	2.15	
5	800	2.5	0.82	300	0	170	9.5	0	3.3	
5	800	2.5	0.61	135	0	125	5.7	0	5.3	
5	800	2.0	0.61	110	0	145	4.6	0	6.1	
5	800	2.0	0.6	92	0	170	3.96	0	4.46	
5	800	2.0	0.43	7.1	71	280	0.418	1.27	10	0.47
5	800	2.0	0.54	69	0	550	3.19	0	16.0	
5	800	2.0	0.9	530	0	640	15.4	0	11.4	
5	800	2.0	0.78	380	0	375	12.6	0	7.6	
5	800	2.0	0.66	205	0	230	8.07	0	5.51	
5	800	2.0	0.54	97	0	205	4.64	0	5.97	0.086
5	800	2.0	0.49	205	0	180	10.8	0	5.8	
5	800	2.0	0.37	6.6	0	1530	0.458	0	65	
5	800	2.0	0.54	35.4	0	380	1.69	0	11.1	0.2
5	800	2.0	0.55	58	0	280	2.69	0	7.9	0.209
5	800	2.0	0.62	80	0	190	3.3	0	4.8	
5	800	2.0	0.41	47	90	740	2.94	1.71	28	0.726
5	800	2.0	0.33	9	520	2200	0.685	12.0	1.02	
5	800	2.0	0.54	54	36	180	2.58	0.52	5.2	

APPENDIX B  
DATA SUMMARY

$P_3$	$T_3$	$\tau_R$	$\phi$	$NO_x$	UHC	CO	$E_{NO_x}$	$E_{HC}$	$E_{CO}$	CI
(atm)	(K)	(msec)		(ppm)	(ppmC)	(ppm)	(g/kg)	(g/kg)	(g/kg)	(%)
5	800	2.0	0.55	46	36	210	2.16	0.515	6.02	0.14
5	800	2.0	0.36	8	45	340	0.57	0.972	14.7	
5	800	2.0	0.38	12	36	160	0.81	0.74	6.6	0.197
5	800	2.0	0.49	13	36	210	0.67	0.57	6.6	0.192
5	800	1.5	0.6	63	60	1140	2.71	0.79	30	
5	800	1.5	0.61	102	0	360	4.3	0	15.1	
5	800	1.0	0.6	52	95	1950	2.24	1.25	51	
5	800	1.0	0.61	114	0	325	4.8	0	13.6	
10	800	3.0	0.57	91.1	8.6	30	4.13		0.83	
10	800	3.0	0.47	32.7	4.3	1	1.77		0.03	
10	800	3.0	0.43	40.2	30.1	10	2.36		0.358	
10	800	3.0	0.51	89.1	25.8	55	4.47		1.68	
10	800	3.0	0.62	239	10.8	105	20.0		2.68	
10	800	3.0	0.63	125	10.8	125	5.13		3.13	
10	800	3.0	0.62	163	5.6	75	6.77		1.9	
10	800	3.0	0.5	57.0	4.3	10	2.93		0.313	
10	800	3.0	0.47	37.2	4.3	1	2.03		0.03	
10	800	3.0	0.4	105	0	120	7.55	0	2.7	
10	800	3.0	0.54	54	0	5	2.58	0	0.44	
10	800	3.0	0.62	87	0	10	3.6	0	3.1	
10	800	3.0	0.57	14.6	0	5	2.1	0	0.3	

43

APPENDIX B  
DATA SUMMARY

$P_3$	$T_3$	$\tau_R$	$\phi$	$NO_x$	UHC	CO	$E_{NO_x}$	$E_{HC}$	$E_{CO}$	CI
(atm)	(K)	(msec)		(ppm)	(ppmC)	(ppm)	(g/kg)	(g/kg)	(g/kg)	(%)
10	800	3.0	0.45	17.3	0	80	0.98	0	2.76	
10	800	2.5	0.71	170	0	100	6.3	0	2.3	
10	800	2.5	0.54	43	0	15	2.06	0	0.44	
10	800	2.5	0.62	60	0	125	2.5	0	3.1	
10	800	2.5	0.57	57	0	9	2.66	0	0.25	
10	800	2.5	0.45	14.9	0	80	0.845	0	2.76	
10	800	2.0	0.71	162	0	80	6.0	0	1.8	0.003
10	800	2.0	0.54	39	0	110	1.87	0	3.2	0.064
10	800	2.0	0.64	33	30	170	1.33	0.37	4.2	
10	800	2.0	0.71	996	0	290	3.68	0	6.5	
10	800	2.0	0.86	290	0	1350	5.82	0	25.2	
10	800	2.0	0.63	30	0	225	1.24	0	5.6	
10	800	2.0	0.63	75	0	250	3.06	0	6.22	
10	800	2.0	0.74	140	0	590	4.9	0	12.7	
10	800	2.0	0.75	178	0	750	6.2	0	15.9	
10	800	2.0	0.55	26	0	105	1.22	0	3.0	
10	800	2.0	0.51	24	0	140	1.2	0	4.3	0.691
10	800	2.0	0.47	25	0	160	1.36	0	5.3	0.105
10	800	2.0	0.38	15	0	162	0.996	0	6.55	0.143
10	800	2.0	0.34	6	0	430	0.45	0	19.5	0.425
10	800	2.0	0.57	52	0	13	2.42	0	0.37	

44



APPENDIX B  
DATA SUMMARY

$P_3$	$T_3$	$\tau_R$	$\phi$	$NO_x$	UHC	CO	$E_{NO_x}$	$E_{HC}$	$E_{CO}$	CI
(atm)	(K)	(msec)		(ppm)	(ppmC)	(ppm)	(g/kg)	(g/kg)	(g/kg)	(%)
10	800	2.0	0.45	9.9	0	80	0.56	0	2.76	
10	800	2.0	0.53	52.2	220	37	0.53	3.25	1.09	
10	800	2.0	0.63	84.5	400	27	3.48	5.03	0.68	
10	800	1.5	0.71	133	0	520	4.9	0	11.7	
10	800	1.5	0.54	5.3	6720	1280	0.25	98	37.3	
10	800	1.5	0.63	13	0	705	0.54	0	17.7	
10	800	1.5	0.57	34	80	13	1.58	1.14	0.37	
10	800	1.5	0.45	4.5	920	80	0.255	15.9	2.76	
10	800	1.0	0.71	18	1600	2400	0.67	18	53.9	
10	800	1.0	0.54	4.7	26300	2700	0.22	380	79	
10	800	1.0	0.63	5	0	1700	0.21	0	42.7	
10	800	1.0	0.45	6.2	10600	80	0.35	183	2.76	
20	800	3.0	0.55	81.8	12.2	30	3.79	0.17	0.85	
20	800	3.0	0.56	84.7	103	60	3.92	1.46	1.69	
20	800	3.0	0.42	18.8	51	0	1.13	0.93	0	
20	800	2.5	0.55	95.6	8.1	35	4.43	0.11	0.99	
20	800	2.5	0.56	147	26.5	10	6.84	0.374	0.28	
20	800	2.5	0.42	16.3	34.6	0	0.98	0.63	0	
20	800	2.0	0.55	99.5	12.2	50	4.61	0.17	1.41	
20	800	2.0	0.56	137	32.6	40	6.36	0.46	1.13	
20	800	2.0	0.42	14.8	32.6	20	0.89	0.60	0.73	

APPENDIX B  
DATA SUMMARY

94

$P_3$	$T_3$	$\tau_R$	$\phi$	$NO_x$	UHC	CO	$E_{NO_x}$	$E_{HC}$	$E_{CO}$	CI
(atm)	(K)	(msec)		(ppm)	(ppmC)	(ppm)	(g/kg)	(g/kg)	(g/kg)	(%)
20	800	2.0	0.68	241	47.3	205	0.68	0.55	4.77	
20	800	2.0	0.57	76.9	51.1	115	0.57	0.699	3.15	0.08
20	800	2.0	0.54	73.7	155	180	0.54	2.27	5.26	0.31
20	800	2.0	0.46	29.1	235	440	0.46	3.99	15.0	0.73
20	800	1.5	0.55	73.9	761	2140	0.55	10.7	60.5	
20	800	1.5	0.56	53.5		2640	0.56		74.5	
20	800	1.0	0.55	34.1	10580	>3000	0.55	149	>85	
20	800	1.0	0.56	20.6	9643	>3000	0.56	136	>85	
30	600	2.0	0.46	29.1	0	1400	1.61	0	47.1	
30	600	2.0	0.52	44.7	0	1240	2.19	0	37.1	
30	800	2.0	0.72	77.6	10.0	20	2.80	0.439	0.439	
30	800	2.0	0.88	196	8.03	100	5.82	1.81	1.81	
30	800	2.0	0.86	193	8.03	45	5.85	0.830	0.830	
30	800	2.0	0.58	50	169	1500	2.23	40.7	40.7	1.1
30	800	2.0	0.64	70	30.1	680	2.81	16.7	16.7	0.301
5	1000	3.0	0.60	248	10.2	60	10.7	0.134	1.58	
5	1000	3.0	0.54	68.5	61	60	3.25	0.88	1.73	
5	1000	2.5	0.60	373	10.2	55	16.1	0.134	1.44	
5	1000	2.5	0.54	68.3	81.4	37.5	3.24	1.18	1.08	
5	1000	2.0	0.52	93.1	12.2	58	4.62	0.185	1.76	
5	1000	2.0	0.49	70.9	10.2	100	3.67	0.161	3.15	

APPENDIX B  
DATA SUMMARY

$P_3$	$T_3$	$\tau_R$	$\phi$	$NO_x$	UHC	CO	$E_{NO_x}$	$E_{HC}$	$E_{CO}$	CI
(atm)	(K)	(msec)		(ppm)	(ppmC)	(ppm)	(g/kg)	(g/kg)	(g/kg)	(%)
5	1000	2.0	0.46	42.9	14.2	190	2.39	0.241	6.44	0.101
5	1000	2.0	0.40	24	16.3	260	1.52	0.314	10.0	0.23
5	1000	2.0	0.35	9.56	16.3	260	0.689	0.358	11.4	0.28
5	1000	2.0	0.35	7	40.7	430	0.514	0.911	19.3	0.51
5	1000	2.0	0.35	5.03	40.7	630	0.368	0.906	28.1	0.706
5	1000	2.0	0.43	26.6	14.2	250	1.59	0.258	9.08	0.188
5	1000	2.0	0.45	38.9	12.2	60	2.22	0.212	2.09	
5	1000	2.0	0.48	67.5	8.14	70	3.62	0.133	2.29	
5	1000	2.0	0.55	177	6.1	60	8.20	0.086	1.69	
5	1000	2.0	0.60	248	8.14	60	10.7	0.11	1.58	
5	1000	2.0	0.60	318	8.14	60	13.7	0.11	1.58	
5	1000	2.0	0.54	61.8	14.2	65	2.93	0.205	1.88	
5	1000	1.5	0.60	91.6	71.2	1010	3.95	0.934	26.5	
5	1000	1.5	0.54	10.5	138	1400	0.498	1.99	40.4	
5	1000	1.0	0.60	16.3	3804	>3000	0.702	49.9	>80	
5	1000	1.0	0.54	12.7	443	>3000	0.602	6.40	>90	
10	1000	1.0	0.55	203	7.6	230	9.40	0.107	6.50	
10	1000	1.0	0.44	25.2	90.8	1210	1.17	42.7	42.7	
10	1000	1.0	0.53	54.6	51.1	810	2.66	24.0	24.0	

47

APPENDIX B  
DATA SUMMARY

$P_3$	$T_3$	$\tau_R$	$\phi$	$NO_x$	UHC	CO	$E_{NO_x}$	$E_{HC}$	$E_{CO}$	CI
(atm)	(K)	(msec)		(ppm)	(ppmC)	(ppm)	(g/kg)	(g/kg)	(g/kg)	(%)
10	1000	3.0	0.55	277	13.2	60	12.8	0.186	1.69	
10	1000	3.0	0.44	9.0	0	0	0.417	0	0	
10	1000	3.0	0.53	196	953	35	9.53	14.1	1.04	
10	1000	2.5	0.55	234	7.6	55	10.9	0.107	1.55	
10	1000	2.5	0.44	27.6	3.78	32	1.28	0.07	1.13	
10	1000	2.5	0.53	121	1456	20	5.90	21.6	0.59	
10	1000	2.0	0.55	177	9.5	160	8.22	0.134	4.52	
10	1000	2.0	0.44	37.0	56.7	280	1.72	1.0	9.87	
10	1000	2.0	0.53	116	265	20	5.65	3.92	0.593	
10	1000	2.0	0.76	1654	170	530	56.5	1.77	11.0	
10	1000	2.0	0.65	483	255	300	19.1	3.06	7.22	
10	1000	2.0	0.56	290	170	280	13.4	2.38	7.86	
10	1000	2.0	0.58	218	115	2020	9.63	1.55	54.5	
10	1000	2.0	0.56	226	76.4	340	10.4	1.07	9.55	0.111
10	1000	2.0	0.44	49.6	2928	320	2.91	52.3	11.4	5.46
10	1000	1.5	0.55	250	26.5	330	11.6	0.374	9.32	
10	1000	1.5	0.44	18.3	284	1280	0.849	5.0	45.1	
10	1000	1.5	0.53	57.3	265	760	2.79	3.92	22.5	

1. Report No. <b>NASA CR-3032</b>	2. Government Accession No.	3. Recipient's Catalog No.	
4. Title and Subtitle <b>EXPERIMENTAL STUDY OF THE EFFECT OF CYCLE PRESSURE ON LEAN COMBUSTION EMISSIONS</b>		5. Report Date <b>July 1978</b>	6. Performing Organization Code
		8. Performing Organization Report No. <b>GASL TR 248</b>	
7. Author(s) <b>Gerald Roffe and K. S. Venkataramani</b>		10. Work Unit No.	11. Contract or Grant No. <b>NAS3-20581</b>
9. Performing Organization Name and Address <b>General Applied Science Laboratories, Inc. Merrick and Stewart Avenues Westbury, New York 11590</b>		13. Type of Report and Period Covered <b>Contractor Report</b>	
		14. Sponsoring Agency Code	
12. Sponsoring Agency Name and Address <b>National Aeronautics and Space Administration Washington, D.C. 20546</b>		15. Supplementary Notes <b>Final report. Project Manager, Gregory M. Reck, Airbreathing Engines Division, NASA Lewis Research Center, Cleveland, Ohio 44135.</b>	
16. Abstract <p>Experiments were conducted in which a stream of premixed propane and air was burned under conditions representative of gas turbine operation. Emissions of <math>\text{NO}_x</math>, CO and unburned hydrocarbons (UHC) were measured over a range of combustor inlet temperature (600 K - 1000 K), pressure (5 atm - 30 atm) and residence time (1 msec - 3 msec) at equivalence ratios from 0.7 down to the lean stability limit. At inlet temperatures of 800 K and 1000 K, <math>\text{NO}_x</math> emissions displayed only moderate sensitivity to pressure. <math>\text{NO}_x</math> emissions at an inlet temperature of 800 K varied approximately as the square root of pressure. At an inlet temperature of 600 K, observed <math>\text{NO}_x</math> levels dropped markedly with decreasing pressure for pressures below 20 atm. <math>\text{NO}_x</math> levels are proportional to combustor residence time and formation rates were principally a function of adiabatic flame temperature. For adiabatic flame temperatures of 2050 K and higher, CO reached chemical equilibrium within 2 msec. Unburned hydrocarbon species dropped to a negligible level within 2 msec regardless of inlet temperature, pressure or equivalence ratio. For a combustor residence time of 2.5 msec, combustion inefficiency became less than 0.01% at an adiabatic flame temperature of 2050 K. The maximum combustion inefficiency observed was on the order of 1% and corresponded to conditions near the lean stability limit. Using a perforated plate flameholder, this limit is well represented by the condition of 1800 K adiabatic flame temperature.</p>			
17. Key Words (Suggested by Author(s)) <b>Lean premixed combustion; Emissions; Oxides of nitrogen; Carbon monoxide; Unburned hydrocarbons; Combustion efficiency</b>		18. Distribution Statement <b>Unclassified - unlimited STAR Category 07</b>	
19. Security Classif. (of this report) <b>Unclassified</b>	20. Security Classif. (of this page) <b>Unclassified</b>	21. No. of Pages <b>50</b>	22. Price* <b>A02</b>

\* For sale by the National Technical Information Service, Springfield, Virginia 22161